American Mineralogist, Volume 92, pages 1881–1898, 2007

Partitioning of trace elements among coexisting crystals, melt, and supercritical fluid during isobaric crystallization and melting

Frank J. Spera,[1,*] Wendy A. Bohrson,[2] Christy B. Till,[3,†] and Mark S. Ghiorso[4]

[1]Department of Earth Science and Institute for Crustal Studies, University of California, Santa Barbara, California 93106, U.S.A.
[2]Department of Geological Sciences, Central Washington University, Ellensburg, Washington 98926, U.S.A.
[3]Department of Earth Science, University of California, Santa Barbara, California 93106, U.S.A.
[4]OFM Research-West, 7336 24th Avenue NE, Seattle, Washington 98115, U.S.A.

Abstract

The distribution of trace elements among coexisting crystals, melt, and supercritical fluid during melting and crystallization is a critical constraint for understanding the evolution of magmatic systems, including the origin and development of continental and oceanic crust. Although trace-element partitioning between crystals and melt during Rayleigh fractional crystallization or melting is well-known, partitioning among co-existing melt, crystals, and supercritical fluid during anatexis or crystallization is less explored despite the ubiquity of magmatic fluids. Here we develop the trace-element differential equations governing solid-melt-fluid equilibria for melting and crystallization under fluid-present conditions and provide analytical solutions for fractional and equilibrium crystallization and melting. A compilation of solid-fluid and melt-fluid distribution coefficients for about 30 trace elements in olivine, clinopyroxene, garnet, plagioclase, alkali feldspar, biotite, amphibole, apatite, and silicic melts is provided. Forward modeling demonstrates the conditions under which fluid-melt-solid partitioning will impact trace-element signatures in magmatic systems. We show that for trace elements soluble in aqueous fluids, the composition of a melt derived by fluid-present fractional crystallization or by fluid-present fractional melting will be significantly different than in otherwise comparable fluid-absent systems. Ignoring the partitioning of soluble elements into the fluid phase leads to large errors in concentrations (over 100%) and ratios and consequent misinterpretation of the trace-element character of source material and/or the processes of fractional crystallization and melting. Although significant in any setting involving fluid-present equilibria, this analysis may have a most profound influence on fluid-present subduction zone magma generation and the evolution of shallow level fluid-saturated silicic magmatic systems.

Keywords: Distribution coefficient, fluid-saturated magma, fluid-melt, solid-melt, trace element

Introduction

Magmatic processes including fractional or equilibrium crystallization or melting under isochoric or isobaric conditions, combined recharge-assimilation-fractionation, isentropic decompression melting, and volatile-fluxed melting are relevant to the eruption and intrusion of about 30 km^3 of magma per year on Earth in various petrotectonic environments (e.g., White et al. 2006). Magmatism is one of the principal mechanisms of mass transfer among terrestrial geochemical reservoirs, and understanding the partitioning of elements during magmatic processes is a keystone for understanding global geochemical cycling. In particular, petrogenesis relies on quantitative analysis of the distribution of trace elements among coexisting crystals, melt, and supercritical fluids during phase transitions such as melting, crystallization, and fluid exsolution. It has been argued that water is essential for the formation of granite and, in turn, granite is essential for the formation of continents. Earth, the only terrestrial planet with abundant water, is the only planet with granitic cratons and continents (Campbell and Taylor 1983). Fluids are ubiquitous in the terrestrial crust and mantle and are essential components of magmatic-hydrothermal systems, which concentrate intrinsically low abundance trace elements (e.g., Cu, Mo, W, Sn, etc.) to form economic mineral deposits (Holland 1972; Burnham 1979; Candela 1989). Fluids also significantly influence magma transport and thermodynamic properties, and have dynamical consequences including contributing to explosive volcanic eruptions. Fluid components are recycled into the upper mantle by subduction of hydrated oceanic crust (sediments and altered mafic crust) and may enter the transition zone and lower mantle (Litasov et al. 2003; Ohtani et al. 2004). Fluids derived from slab dehydration exert important constraints on the trace-element signatures of melts generated by anatexis of metasomatized (carbonated and hydrated) peridotite (McCulloch and Gamble 1991; Plank and Langmuir 1998; Stern 2002; Elliott 2003; Kelemen et al. 2003; Tatsumi 2005) or subducted lithospheric sources (Defant and Drummond 1990). Prouteau et al. (1999) have argued that slab melting in modern subduction zones occurs under fluid-present conditions at tem-

* E-mail: spera@geol.ucsb.edu
† Present address: Earth, Atmospheric and Planetary Sciences, Massachusetts Institute of Technology, Cambridge, MA 02139, U.S.A.

0003-004X/07/1112–1881$05.00/DOI: 10.2138/am.2007.2326

peratures below 900 °C, in agreement with thermal regimes deduced from fluid dynamical calculations. An important role for water has been suggested in komatiite genesis in the Archean and Proterozoic (Grove and Parman 2004). In the crust, partial melting of hydroxyl-bearing source rocks under fluid-present conditions (e.g., Berger et al. 2006) and ubiquitous low-pressure, volatile-saturated fractional crystallization are scenarios for which solid-melt-fluid trace-element partitioning is important, perhaps critically so.

Despite the ubiquity of fluids in magmatic systems, trace-element partitioning in solid-fluid-melt multiphase systems has not been treated in much detail probably for two reasons: (1) until recently, very few data on solid-fluid trace-element partition coefficients were available, and (2) a rigorous and easy-to-implement formulation applicable to both fractional melting and fractional crystallization applicable to fluid-present processes has not been available. Previous work on fluid-present fractional crystallization invoked an approximation in which the mass fraction of the fluid phase was ignored in the mass-balance expression (Allègre et al. 1977). This procedure is generally invalid, especially in multiphase systems in which the fraction of fluid (f_f) exceeds ≈0.05. Likewise, the model for fractional melting developed by Shaw (1978) assumed that the ratio of fluid to solid mass in the residue was constant during progressive fractional melting. However, because H_2O and other volatiles are appreciably soluble in melts, the process of fractional fusion leads to progressive dehydration of the residue, and thus the mass ratio of fluid to solid is not at all constant but instead sharply decreases.

The main purpose of this work is to present derivations of the mass-balance relations for calculation of trace-element concentrations in coexisting phases in fluid-present multiphase systems subject to either equilibrium or fractional partial melting or crystallization. The term "fluid present" means that during the process of fractional crystallization (FC) or fractional melting (FM), a distinct fluid phase is present. The H_2O component, of course, is distributed assuming thermodynamic local equilibrium between all phases present. If H_2O is the only volatile component, then the fugacity of H_2O in the fluid phase is identical to the fugacity of pure H_2O at the conditions of pressure and temperature at which FC or FM takes place. In the FC model, phases that exsolve (e.g., water bubbles) or crystallize (phenocrysts) from the liquid are instantaneously and completely removed; they cannot back react with the melt. In the FM model, the melt phase is instantaneously and completely removed during partial melting. The melt is assumed not to carry away the fluid phase (e.g., fluid bubbles) although the melt will contain significant amounts of dissolved H_2O. Progressive partial melting is therefore an efficient process to dehydrate source materials due to the relatively large solubility of H_2O in typical crustal and mantle melts. If the assumption is made that during FM the fluid phase is indeed removed along with volatile-saturated melt (e.g., as discrete fluid bubbles), then there can never be a condition of fluid-present partial melting. We also present a compilation of experimentally determined solid-fluid trace-element partition coefficients to facilitate geochemical computations. This paper is organized as follows: after a review of previous work, a model for trace-element partitioning in solid-melt-fluid systems is offered. In particular, we derive the differential mass-balance relations governing the partitioning of trace elements among bulk solid, melt, and fluid phases during isobaric fractional melting and isobaric fractional crystallization. In general, the derived differential equations must be solved numerically to account for the variation of partition coefficients, fluid mass fraction (f_f) and water solubility in melt with melt fraction (f_m), temperature, and melt and fluid composition. Trace-element evolution is formulated as a coupled set of differential equations: one represents the material balance for the trace element and the other a material balance for the H_2O component in a mixed-volatile system. In the simplified case when (1) the solid-fluid (K_{sf}) and solid-melt (K_{sm}) partition coefficients are constant; (2) H_2O is the only volatile constituent; and (3) the water solubility depends only on pressure, an analytical solution may be found. Comparison of the fluid-present solutions to those of an otherwise identical fluid-absent system reveals large differences for elements with solid-fluid partition coefficients $K_{sf} \leq 1$. Solutions are also given for equilibrium melting and equilibrium crystallization (Appendix IV). A compilation of mineral-fluid and melt-fluid partition coefficients is presented in Electronic Appendix 1[1] to facilitate trace-element analysis in fluid-present systems. The critical conclusion of this work is that for many low-field-strength (soluble) elements, predicted trace-element concentrations and ratios in the melt are quite different compared to otherwise identical, but fluid-absent, cases. The ubiquity of fluid-saturated systems implies that fluid-present equations should be applicable to many magmatic systems.

Previous work: Fluid-present fractional crystallization and fractional melting

The distribution of trace elements between crystals and melt in magmatic systems governed by Rayleigh fractional crystallization has long been a topic of intense geochemical interest (e.g., Gast 1968; Schilling and Winchester 1967; Allègre et al. 1977; Allègre and Minster 1978; Minster et al. 1977; Albarède 1995). The more general case of fluid-present solidification—that is, fractional crystallization of a fluid-saturated melt—has received far less attention, despite the ubiquity of fluids in magmatic systems. Virtually all erupted magmas are fluid saturated, a consequence of the very low solubility of water (and most other volatile species) at low pressure and the strong dependence of water solubility upon pressure. Significantly, experimental data show that some trace elements are strongly fractionated into a supercritical aqueous fluid phase relative to coexisting solids and melt (e.g., Brenan et al. 1995; Keppler 1996; Stalder et al. 1998; Kessel et al. 2005; see Electronic Appendix 1 for many additional references and database), thus clearly establishing the relevance of fluid-present, trace-element fractional crystallization. Earlier work on this problem by Allègre et al. (1977)

[1] Deposit item AM-07-034, Electronic Appendix 1 (a compilation of mineral-fluid and melt-fluid partition coefficients). Deposit items are available two ways: For a paper copy contact the Business Office of the Mineralogical Society of America (see inside front cover of recent issue) for price information. For an electronic copy visit the MSA web site at http://www.minsocam.org, go to the American Mineralogist Contents, find the table of contents for the specific volume/issue wanted, and then click on the deposit link there.

explicitly made the approximation of neglecting the presence of the fluid phase in the material-balance expression. Although this assumption is reasonable for very dry magmas (<0.5 wt% H_2O) at high pressure, it introduces large errors when applied to relatively soluble low-field-strength elements in typical hydrous magmatic systems. In fact, this assumption is unnecessary if proper accounting of the magma water budget is made. In Appendix I, the derivation of Allègre et al. (1977) is presented and compared to the different formulation developed in this study. In fact, Allègre et al. (1977) did not perform any trace-element calculations of fluid-present fractional crystallization because in their words "such calculations are impossible because we do not know the values of the solid-fluid partition coefficient…" (p. 65). In the intervening thirty years, the situation has changed dramatically, and it is now appropriate to develop a model that can be used in geochemical calculations.

Turning now to fractional melting in the presence of a fluid phase, we note that Shaw (1978) addressed this problem thirty years ago. He assumed that during progressive partial melting, the mass ratio of fluid to solid in the residue is constant. This is often a poor assumption. Because H_2O is rather soluble in natural melts, the effect of melt removal during fractional melting is to dehydrate the residue. The ratio of fluid to solid mass in the residual solid is not constant during progressive partial melting as assumed in the Shaw formulation. To our knowledge, there is no quantitative model for predicting trace-element concentrations in melt, fluid, and residual solids during fluid-present anatexis that accounts for the progressive removal of water (i.e., dehydration) from the source region that accompanies escaping melt. In sum, the geochemical consequences of fluid-present crystallization and fluid-present partial melting have not been examined in adequate detail. The aim of this work is to remedy this situation.

Isobaric fractional crystallization under fluid-saturated conditions

Background

The distribution of minor and trace elements between coexisting phases in fractional crystallization depends on the phase proportions (i.e., fluid, melt, and solid abundances), on the equilibrium partitioning behavior between solid-melt ($K_{sm} = C_s/C_m$) and solid-fluid ($K_{sf} = C_s/C_f$) and on the solubility of water in the melt. The water solubility in turn depends upon the temperature, pressure, and melt and fluid composition. There are alternative but equivalent ways of writing partition coefficients in multiphase systems. Here we choose K_{sm} and K_{sf} because most experimental results are couched in these terms (see Electronic Appendix I). Conversion to other forms, such as the melt-fluid partition coefficient, is accomplished using the identity $K_{mf} = K_{sf}/K_{sm}$. It is widely appreciated that bulk partition coefficients change during progressive crystallization due to variations in the abundance and composition of solids. The phase assemblage, water solubility, and mass fractions of melt (f_m) and fluid (f_f) depend, in turn, upon thermodynamic parameters such as temperature, pressure, system bulk composition, and oxygen fugacity. Hence, the prediction of trace-element distributions demands accurate knowledge of the relevant phase equilibria. Examination of experimental solid-fluid and melt-fluid partition coefficients for volumetrically important phases (e.g., olivine, garnet, clinopyroxene, plagioclase, alkali feldspar, micas, apatite) in equilibrium with aqueous fluids indicates that bulk solid-fluid (K_{sf}) partition coefficients can be small, significantly <0.1. This means that these elements are appreciably soluble in supercritical aqueous fluids, and even if incompatible, they are not necessarily sequestered into melt but instead into coexisting fluid. Consequently, the concentration in the melt of two equally incompatible or compatible elements (i.e., similar K_{sm}), of different solubility in coexisting supercritical fluid (i.e., different K_{sf}), can be very different in fluid-present compared to fluid-absent crystallization. Below a derivation of the differential expressions for trace-element abundance in systems undergoing isobaric fractional crystallization in the presence of a fluid phase is presented.

Mass-balance derivation

Consider a mass M_m^o of a single-phase multicomponent silicate melt subject to closed-system, isobaric fractional crystallization by removal of heat. At any temperature (or enthalpy), the multiphase mixture of crystals (s), melt (m), and supercritical fluid (f) sums to the total initial mass of the system. That is

$$M_S + M_m + M_f = M_m^o \tag{1}$$

or in differential terms

$$dM_s + dM_m + dM_f = 0. \tag{2}$$

For the i^{th} trace element of mass m_i, the analogous expressions are:

$$m_{s,i} + m_{m,i} + m_{f,i} = m_{m,i}^o = C_{m,i}^o M_{m,i}^o \tag{3}$$

and

$$dm_{s,i} + dm_{f,i} + dm_{m,i} = 0. \tag{4}$$

The subscript "i" refers to the i^{th} trace element and is dropped hereafter; the superscript "o" refers to the initial conditions. To obtain the differential balance, allow for an increment of change in which dm_s of a trace element is removed from the melt due to solid formation by fractional crystallization and simultaneously dm_f is removed from melt by fluid exsolution into a coexisting supercritical fluid phase. The concentrations of trace element in the solid and fluid phases are C_s and C_f, respectively, at the instant of removal. Then Equation 4 is written:

$$dm_s + dm_f = -dm_m = -d(C_m M_m) \tag{5}$$

or

$$C_m dM_m + M_m dC_m = -C_s dM_s - C_f dM_f. \tag{6}$$

In Equation 6, the instantaneous concentrations of s trace element in precipitated solid and exsolved fluid are given by

$$C_s = \frac{dm_s}{dM_s} = C_m K_{sm} \tag{7}$$

and

$$C_f = \frac{dm_f}{dM_f} = \frac{C_s}{K_{sf}} = C_m \frac{K_{sm}}{K_{sf}} \tag{8}$$

respectively. Equations 7 and 8 also define the bulk solid-melt (K_{sm}) and solid-fluid (K_{sf}) partition coefficients, respectively. Mass in Equation 6 can be converted to mass fraction using the definition:

$$f_m = \frac{M_m}{M_m + M_f + M_s} = \frac{M_m}{M_m^o}. \tag{9}$$

Analogous expressions for f_f, the mass fraction of supercritical fluid and f_s, the mass fraction of solid, are similarly defined. Upon introduction of the equilibrium bulk solid/melt and bulk solid/fluid partition coefficients ($K_{sm} \equiv C_s/C_m$ and $K_{sf} \equiv C_s/C_f$, respectively), Equation 6 is:

$$\frac{dC_m}{df_m} = \left(K_{sm}(1 - K_{sf}^{-1}) \frac{df_f}{df_m} + (K_{sm} - 1) \right) \frac{C_m}{f_m} \tag{10}$$

or, equivalently,

$$\frac{d \ln C_m}{d \ln f_m} = K_{sm}(1 - K_{sf}^{-1}) \frac{df_f}{df_m} + (K_{sm} - 1). \tag{11}$$

To determine the variation of trace-element concentration in the melt during fractional crystallization, the total derivative of the mass fraction of fluid with respect to mass fraction of melt must be specified. In general, this derivative depends on temperature, pressure, and the bulk composition of the system (including the volatile constituents and their partitioning between melt and fluid), and must be independently determined from a thermodynamic model. To define the derivative of fluid fraction with respect to melt fraction in Equation 11, a material balance on H_2O component in a fluid-present, mixed-volatile system undergoing isobaric fractionation can be invoked. This leads to:

$$Z_w^o = f_m S_w(T, X_m, X_f) + w_w^f f_f \tag{12}$$

where Z_w^o is the initial mass fraction of the H_2O component in the system (a constant), f_m is the mass fraction of melt, S_w is the solubilty of water in the melt (a function of temperature, melt composition, and fluid composition), f_f is the mass fraction of fluid in the system, and w_w^f is the mass fraction of H_2O in the mixed-volatile fluid phase. The derivative of the fluid fraction with respect to the melt fraction can be found from Equation 12 once the solubility function and variation of fluid-phase composition with melt fraction are specified:

$$\frac{df_f}{df_m} = -\left(Z_w^o + S_w^m f_m \right) \frac{d \ln w_w^m}{df_m} - \left(\frac{f_m}{w_w^m} \right) \frac{dS_w^m}{df_m} - \frac{S_w^m}{w_w^m}. \tag{13}$$

The right hand side (RHS) of Equation 13, and hence Equation 10, is not constant due to the dependence of water solubility on temperature, melt, and fluid composition, and because the fluid composition varies during progressive crystallization. In fluid-present fractional crystallization, even when the mass ratio of precipitating solids is constant (e.g., at the eutectic), the RHS of Equation 10 cannot be written in terms of a bulk solid-melt-fluid constant partition coefficient because of the complications induced by the presence of a fluid phase embodied in Equation 13. Fluid-present, trace-element analysis is, therefore, fundamentally different than that for solid-melt trace-element partitioning.

There are instructive special circumstances for which a simpler treatment may be found. In systems where (1) all solid-melt and solid-fluid partition coefficients are constant; (2) only one volatile constituent is considered (e.g., H_2O); and (3) the solubility of water is independent of temperature and system composition, then, and only then, Equation 13 reduces to $\frac{df_f}{df_m} = -S_w^m = \phi$ with φ equal to a constant. These assumptions enable one to determine an explicit analytical solution to Equation 10 and hence gain a basic understanding of the systematics of trace-element distribution in magma that is initially (or becomes) water-saturated during the course of crystallization. In applications to natural geochemical systems, the validity of the aforementioned assumptions should be assessed. The relationship of this simplified case to the standard bulk partition coefficient approach in multiple solid-melt trace element analysis is explored in Appendix II.

Solution of Mass-Balance Equation and Error Analysis

For constant K_{sm}, K_{sf}, and $\varphi \equiv df_f/df_m$, the coupled solution of Equations 13 and 10 is obtained by straightforward integration. The initial condition at the liquidus temperature ($f_s \to 0$) is $C_m = C_m^o$ at $f_m = f_m^o$. The concentration of a trace element in the two-phase (melt plus fluid) system, C_{sys} is related to the phase fractions and trace-element concentrations according to $C_{sys} = f_m^o C_m^o + (1 - f_m^o) \frac{K_{sm}}{K_{sf}} C_m^o$. It follows that the initial amount and concentration of a trace element in the fluid are $f_f^o = 1 - f_m^o$ and $C_f^o = \frac{K_{sm}}{K_{sf}} C_m^o$, respectively. In the case where the melt is just saturated (trace of fluid phase), then $f_m^o = 1$, $C_{sys} = C_m^o$, and $f_f^o = 0$. The physical significance of φ is established by performing a material balance on the H_2O component. This gives $Z_{H_2O}^o + f_m \varphi_{H_2O} = f_f$, where $Z_{H_2O}^o$ is the initial mass fraction of H_2O component in the system and φ_{H_2O} is the negative of the solubility of water in the melt. The solution to Equation 10 for the concentration of trace element in the melt (C_m) and derivative expressions for the instantaneous and average composition of bulk solid (C_s and $\hat{C}_s$) and fluid (C_f and $\hat{C}_f$) are:

$$\frac{C_m}{C_m^o} = \left(\frac{f_m}{f_m^o} \right)^{K_{sm}(1 - K_{sf}^{-1})\phi + K_{sm} - 1} \tag{14}$$

$$\frac{C_s}{C_m^o} = K_{sm} \left(\frac{f_m}{f_m^o} \right)^{K_{sm}(1 - K_{sf}^{-1})\phi + K_{sm} - 1} \tag{15}$$

$$\frac{\hat{C}_s}{C_m^o} = (f_m - f_m^o)^{-1} [(1 - K_{sf}^{-1})\phi + 1]^{-1} \left\{ \left(\frac{f_m}{f_m^o} \right)^{K_{sm}[(1 - K_{sf}^{-1})\phi + 1]} - 1 \right\} \tag{16}$$

$$\frac{C_f}{C_m^o} = \frac{K_{sm}}{K_{sf}} \left(\frac{f_m}{f_m^o} \right)^{K_{sm}(1 - K_{sf}^{-1})\phi + K_{sm} - 1} \tag{17}$$

$$\frac{\hat{C}_f}{C_m^o} = K_{sf}^{-1} (f_m - f_m^o)^{-1} [(1 - K_{sf}^{-1})\phi + 1]^{-1} \left\{ \left(\frac{f_m}{f_m^o} \right)^{K_{sm}[(1 - K_{sf}^{-1})\phi + 1]} - 1 \right\} \tag{18}$$

The average composition of solid and fluid ($\hat{C}_s$ and $\hat{C}_f$, respectively) refers to the mean composition of solid or fluid removed from the melt over the crystallization interval. Note that in the

fluid-absent case ($\varphi = 0$; $f_m^o = 1$), Equation 14 reduces to the classical Rayleigh solid-melt fractionation expression:

$$\frac{C_m}{C_m^o} = f_m^{(K_{sm}-1)} \tag{19}$$

When a fluid phase is present, the concentration of a trace element in the melt depends upon K_{sm}, K_{sf}, and $\varphi = df_f/df_m$. The effect of ignoring partitioning of a trace element into the fluid on the concentration of that the element in the melt can be determined by finding the fractional error using Equations 14 and 19. If a fluid phase is present and has been ignored, then the fractional error in the calculated melt composition is

$$\frac{C_m^{3\Psi} - C_m^{2\Psi}}{C_m^{3\Psi}} = 1 - f_m^{-K_{sm}(1-K_{sf}^{-1})\phi}\left(f_m^o\right)^{K_{sm}-1-K_{sm}(1-K_{sf}^{-1})\phi} \tag{20}$$

where $C_m^{3\Psi}$ and $C_m^{2\Psi}$ represent the fluid-present melt composition and the fluid-absent melt composition, respectively. If it is assumed that melt is just water-saturated at the liquidus, then $f_m^o = 1$ and the last factor on the RHS of Equation 20 is unity. From Equation 20, if K_{sf} is small (i.e., a trace element is soluble) and for typical fluid contents ($\varphi \sim -0.05$), the error can be quite large. In Figure 1, the percent error in the absolute value of the concentration of a trace element in the melt is shown as a function of K_{sm} and K_{sf}. Specifics of the calculations are provided in the figure caption. The striking observation related to Figure 1 is how large the errors are for $K_{sf} < 1$. For example, for an element with $K_{sm} = 1$, errors from ~30% to >100% occur for $K_{sf} \leq 0.1$, which, as we demonstrate in another section, is a reasonable K_{sf} for many soluble elements in typical silicate systems. For a soluble but relatively compatible element, most of the element is in the fluid relative to coexisting melt and solid. Neglecting the existence of the fluid phase in such a case will lead to erroneous

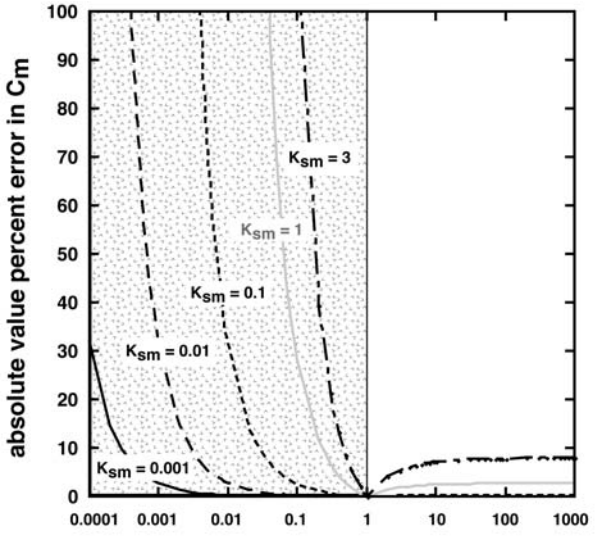

FIGURE 1. Error analysis for fractional crystallization plots bulk K_{sf} vs. absolute value percent error in C_m, based on Equation 20. Results shown for $f_m = 0.5$ (50% fractional crystallization); $\varphi = -0.04$ (4% H_2O at $f_m = 0$); range of K_{sm} from 0.001 to 3. Stippled region denotes negative values of percent error (i.e., $C_m^{3\Psi} < C_m^{2\Psi}$). Note that percent error for $K_{sf} = 1$ is 0 for all K_{sm}. Thus, $K_{sf} = 1$ yields solution that is equivalent to fluid-absent conditions.

conclusions. At the end stages of fractional crystallization, water saturation is a typical condition especially at shallow depth and hence Equations 14–18 are applicable.

The relationships derived above are valid when multiple solid phases are involved in isobaric fractionation, if the bulk partition coefficients:

$$\bar{K}_{sm} = \sum_i^n w_i K_{sm}^i \tag{21}$$

and

$$\bar{K}_{sf} = \sum_i^n w_i K_{sf}^i \tag{22}$$

(where w_i is the mass fraction of the i^{th} phase in the assemblage at some particular f_m) are used to replace K_{sm} and K_{sf} in Equations 14–18.

Scale analysis

It is useful to categorize the behavior of a trace element according to both its partitioning between solid and melt (i.e., its incompatibility) and its partitioning between solid and fluid (i.e., its solubility). The melt-fluid partition coefficient K_{mf} ($\equiv C_m/C_f = K_{sf}/K_{sm}$) is smallest for soluble, compatible elements, and greatest for insoluble, incompatible elements. Unlike the case in fluid-absent crystallization, the concentration of an incompatible element in the melt during solidification can either increase or decrease depending on the values of K_{sm}, K_{sf}, and φ. To simplify the discussion, in reference to Equation 14, we define $A = K_{sm}(1 - K_{sf}^{-1})$ and $B = K_{sm} - 1$. These parameters determine the sign and magnitude of $A\varphi + B$, the exponent in Equation 14. Here, we establish the categories for solid-melt partitioning of very incompatible ($K_{sm} < 10^{-3}$), moderately incompatible ($K_{sm} \approx 10^{-1}$), compatible ($K_{sm} \approx 1$), and very compatible ($K_{sm} > 3$) elements and for solid-fluid partitioning of very soluble ($K_{sf} < 10^{-4}$), soluble ($K_{sf} \approx 10^{-2}$), moderately soluble ($K_{sf} \approx 1$), and insoluble ($K_{sf} > 100$) elements. An element in a specific phase in equilibrium with a particular melt can be roughly categorized depending upon temperature, pressure, oxygen fugacity, bulk condensed phase composition, and fluid-phase composition. Scale analysis of Equation 14 allows one to determine geochemical partitioning in asymptotically limiting situations. Consider, for example, a group of elements, all of which are incompatible ($K_{sm} = 10^{-2}$) but of varying solubility (e.g., K_{sf} from 10^{-4} to 100). For a soluble but incompatible element, the sum $A\varphi + B \rightarrow -(1 + \varphi K_{sm}/K_{sf})$ whereas for an insoluble but incompatible element, the sum $A\varphi + B \rightarrow \varphi K_{sm} - 1$. For a very incompatible, insoluble element, $A\varphi + B \rightarrow -1$ and the classical Rayleigh fractionation result, $\frac{C_m}{C_m^o} = f_m^{-1}$, is recovered. In contrast, for a compatible element of varying solubility, limiting values for $A\varphi + B$ are $-\varphi K_{sm}/K_{sf}$ for high-solubility elements, and φK_{sm} for insoluble ones. These and other limiting forms for $A\varphi + B$ are summarized in Table 1.

Graphical results

Solution to Equation 14 is presented in Figures 2 and 3 for a range of K_{sm} and K_{sf}, and for melts of different (but petrologically typical) water solubility (recall $S_w = -\varphi$). The curves give the normalized concentration, C_m/C_m^o for K_{sf} values spanning the range of behaviors from incompatible to compatible. To obtain

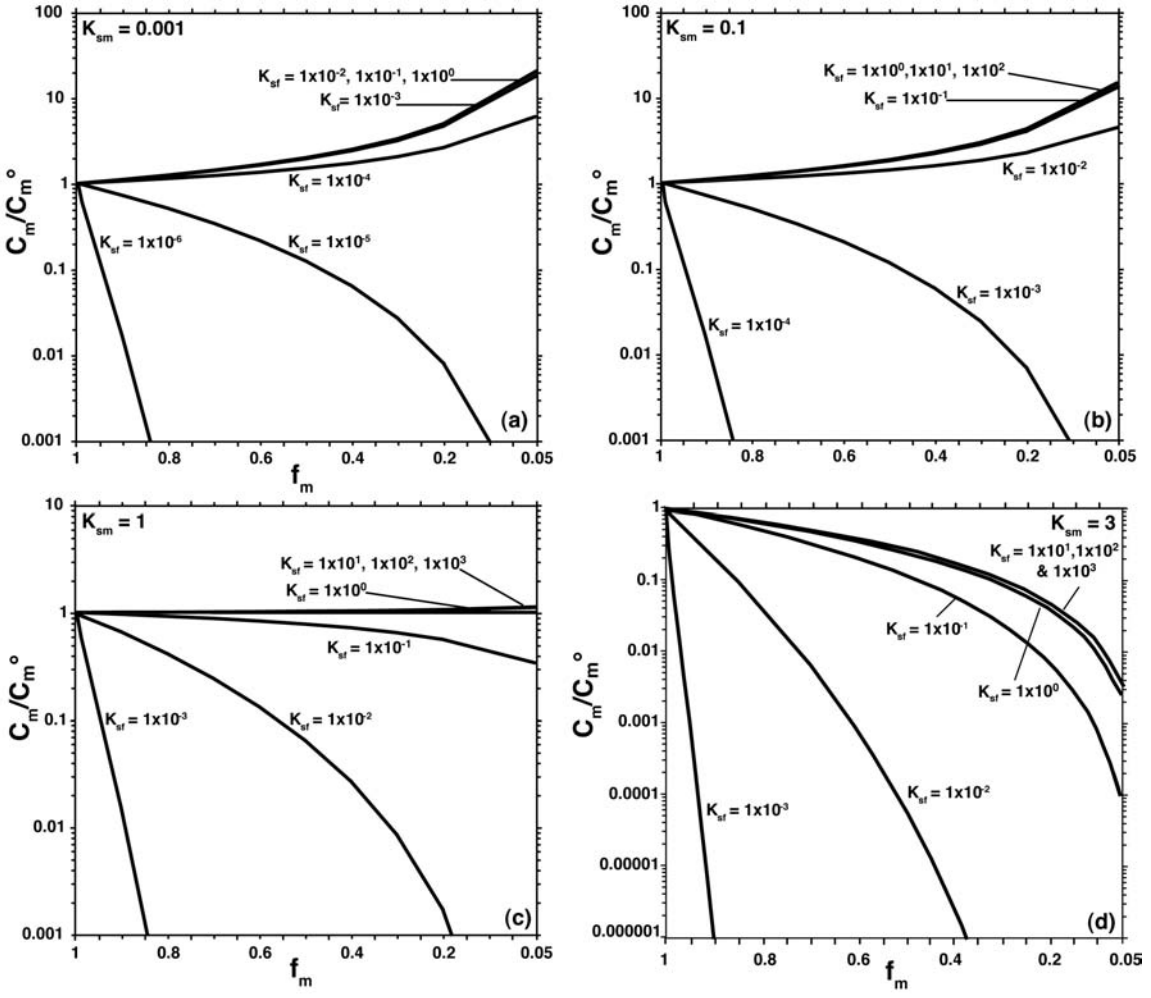

FIGURE 2. Plots depicting behavior of normalized trace-element concentration (C_m/C_m^o) vs. f_m for fractional crystallization; φ = –0.04. In all plots, K_{sf} = 1 illustrates system behavior for fluid-absent conditions. (**a**) Curves illustrating C_m/C_m^o trends for K_{sm} = 0.001 and $K_{sf\ of}$ 10^{-6} to 1. (**b**) K_{sm} = 0.1 and K_{sf} of 10^{-4} to 100. (**c**) K_{sm} = 1.0 and K_{sf} of 10^{-3} to 1000. (**d**) K_{sm} = 3 and K_{sf} of 10^{-3} to 1000. Calculations stopped at f_m = 0.05.

TABLE 1. Scale analysis

	Very Incompatible $K_{sm} < 10^{-3}$	Moderately Incompatible $K_{sm} \approx 10^{-1}$	Compatible $K_{sm} \approx 1$	Very Compatible $K_{sm} > 3$
Very Soluble $K_{sf} < 10^{-4}$	$-[(K_{sm}/K_{sf})\varphi + 1]$	$-[(K_{sm}/K_{sf})\varphi + 1]$	$(-K_{sm}/K_{sf})\varphi$	$K_{sm}(1 - \varphi/K_{sf})$
Soluble $K_{sf} \approx 10^{-2}$	$-[(K_{sm}/K_{sf})\varphi + 1]$	$-[(K_{sm}/K_{sf})\varphi + 1]$	$(-K_{sm}/K_{sf})\varphi$	$K_{sm}(1 - \varphi/K_{sf})$
Moderately Soluble $K_{sf} \approx 1$	$K_{sm}\varphi - 1$	$K_{sm}\varphi - 1$	$K_{sm}\varphi$	$K_{sm}(\varphi + 1)$
Insoluble $K_{sf} > 100$	–1	$K_{sm}\varphi - 1$	$K_{sm}\varphi$	$K_{sm}(\varphi + 1)$

solutions, values of the derivative $\varphi = df_f/df_m$ are needed. Based on the concentration of H_2O in common magmas, reasonable values for $\varphi = df_f/df_m$ are $-0.1 < \varphi < -0.01$. This range is consistent with H_2O abundances from 1 to 10 wt% in common primary magmas; smaller (i.e., more negative) values are expected for "wet" magmas characteristic of silicic systems. In Figure 2, φ is set equal to –0.04, appropriate for a moderately wet parental magma initially containing 4 wt% dissolved H_2O ($Z_w^o = 0.04$), whereas in Figure 3, φ equals –0.08, a value appropriate for "wet" compositionally evolved magmas (~8 wt% initial H_2O). In isobaric fractional crystallization, other than a small amount of H_2O bound in hydrous phenocrysts (e.g., biotite, amphibole, apatite, etc.), most of the H_2O is exsolved from the melt and removed via "second boiling."

Relations are shown for four values of K_{sm} ranging from incompatible (0.001, 0.1) to compatible (1,3). C_m/C_m^o is plotted vs. melt fraction (f_m) in the multiphase (solid + melt + fluid) magmatic mixture. For φ = –0.04, the impact that fluid-present conditions has on the trace-element signatures varies and depends on K_{sm}. For a highly incompatible element (K_{sm} = 0.001), the element must be highly soluble ($K_{sf} > 10^{-4}$) to generate a substantial deviation from fluid-absent signatures (Fig. 2a). In all plots, K_{sf} = 1 illustrates system behavior for fluid-absent conditions. Deviations occur for cases in which $K_{sf} < 0.01$ for moderately incompatible elements (Fig. 2b); for example, at 50% crystallization, a system with K_{sm} = 0.1 and $K_{sf} = 10^{-3}$, fluid-present conditions would yield more than an order-of-magnitude lower trace-element concentration, relative to fluid-absent conditions. For a fluid-saturated melt that has only olivine or olivine and clinopyroxene as liquidus phases, fractional crystallization has

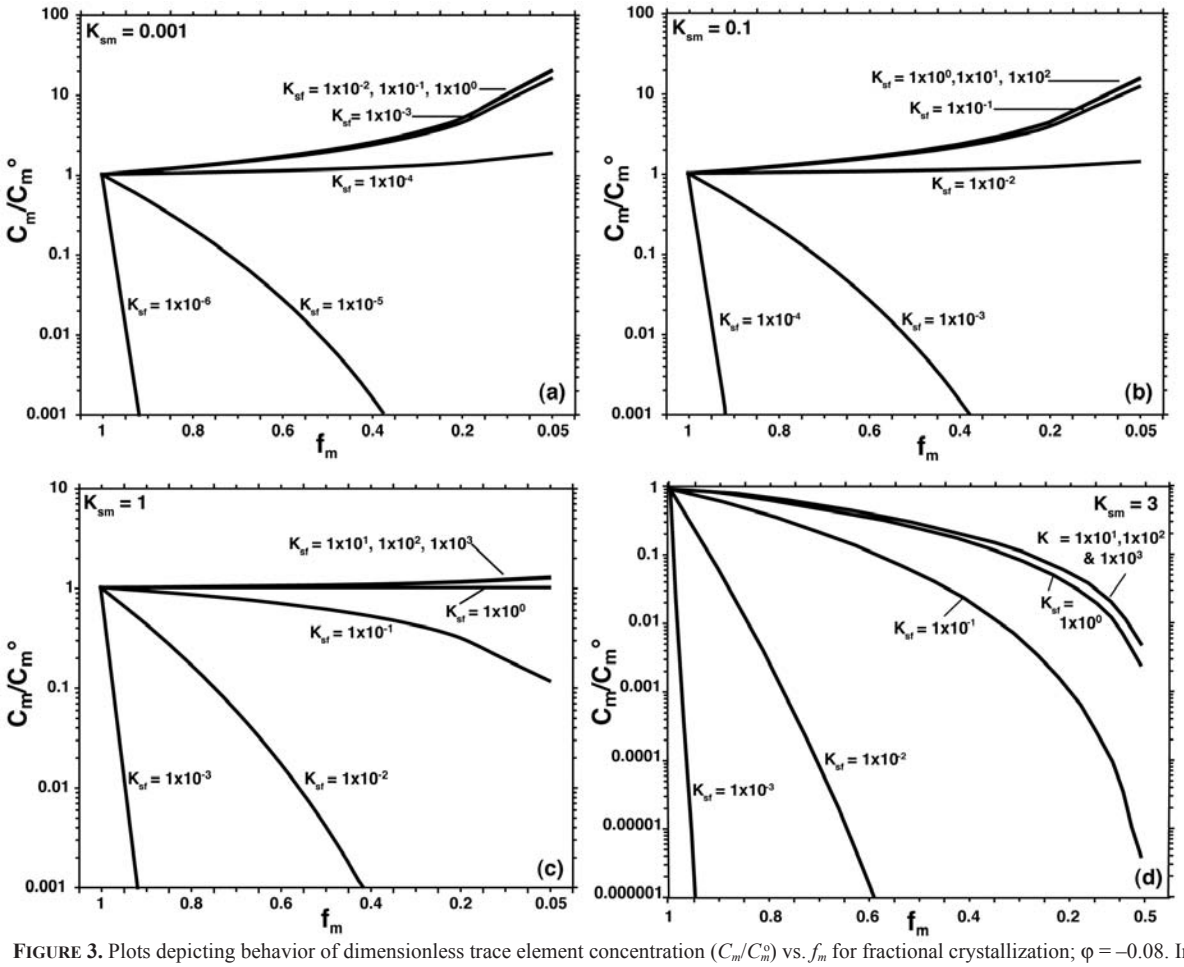

FIGURE 3. Plots depicting behavior of dimensionless trace element concentration (C_m/C_m^o) vs. f_m for fractional crystallization; φ = –0.08. In all plots, K_{sf} = 1 illustrates system behavior for fluid-absent conditions. (**a**) Curves illustrating C_m/C_m^o trends for K_{sm} = 0.001 and K_{sf} of 10^{-6} to 1. (**b**) K_{sm} = 0.1 and K_{sf} of 10^{-4} to 100. (**c**) K_{sm} = 1.0 and K_{sf} of 10^{-3} to 1000. (**d**) K_{sm} = 3 and K_{sf} of 10^{-3} to 1000. Calculations stopped at f_m = 0.05.

the potential to change concentrations of elements such as Rb, Sr, Pb, and U relative to less-soluble ones such as many of the REE, Zr, or Nb. For compatible elements, discernible differences can be seen at K_{sf} as large as 10^{-2}. For example, an element characterized by K_{sm} = 1 and K_{sf} = 10^{-2}, fluid-present conditions of φ ≈ –0.04 would yield slightly more than an order-of-magnitude lower trace-element concentration, relative to fluid-absent conditions.

In Figures 3a–3d, the normalized concentration of a trace element in the melt is shown for a parental melt containing 8 wt% H_2O (φ = df_f/df_m = –0.08). Relations are shown for the same set of values of K_{sm} as in Figure 2. Comparison of Figures 2 and 3 shows that the higher fluid content magnifies the differences in trace-element concentration, as expected. For example, for K_{sm} = 0.1 and K_{sf} = 10^{-3}, 50% crystallization yields approximately an order-of-magnitude lower normalized concentration, compared to the φ = –0.04 case, and two orders of magnitude lower than the fluid-absent case.

From these simple calculations, it is clear that assessing the role of fluids in trace-element balance is essential during fluid-present fractional crystallization. There have been hundreds of cases of fractional crystallization for petrologic systems presented in the literature in the past 30 years. To our knowledge, few of these studies have explicitly considered the effect of simultaneous solid-fluid-melt trace-element partitioning, despite the fact that fluid-saturation during fractional crystallization is common. For very insoluble elements, neglect of fluids is less egregious although small errors can still be incurred. For soluble elements, lack of consideration of fluids renders any analysis inchoate at best.

ISOBARIC FRACTIONAL MELTING UNDER FLUID-SATURATED CONDITIONS

Mass-balance derivation

Consider a system, initially composed of multiple solid phases of total mass (M_s^o) and a single fluid phase (M_f^o) subject to fractional melting under isobaric conditions. In fractional melting, silicate melt generated by partial melting is immediately and completely removed from the system. Although the fluid phase remains in the residue, fluid components will be removed from the system due to progressive removal of fluid-saturated melt. Our interest is in calculating the concentration of a trace element in successive aliquots of melt during fractional melting. We do this by first calculating the concentration of a trace element in the residual solid

(or bulk solid) and then use the definition of the solid-melt partition coefficient to compute the concentration in the melt aliquot as a function of the fraction of melt removed (f_m).

At any temperature, the multiphase mixture of crystals (s), melt (m), and supercritical fluid (f) sums to the total initial mass of the system. That is:

$$M_s + M_m + M_f = M_s^o + M_f^o \tag{23}$$

or in differential terms

$$dM_s + dM_m + dM_f = 0. \tag{24}$$

For the i^{th} trace element of mass m_i, the analogous expressions are

$$m_{s,i} + m_{m,i} + m_{f,i} = m_{s,i}^o + m_{f,i}^o = C_{s,i}^o M_{s,i}^o + C_{f,i}^o M_{f,i}^o \tag{25}$$

and

$$dm_{s,i} + dm_{f,i} = -dm_{m,i}. \tag{26}$$

The subscript "i" refers to the i^{th} trace element and is dropped hereafter; the superscript "o" refers to the initial conditions. To obtain the differential balance, allow for an increment of change in which a mass increment of a trace element is removed from the initial source material (solid plus fluid) by the removal of melt implied by fractional fusion. The concentration of a trace element in the melt is C_m at the moment of melt removal. Then Equation 26 can be cast as

$$d(C_s M_s + C_f M_f) = -dm_m = -C_m dM_m \tag{27}$$

Now, if the definitions $C_m = C_s K_{sm}^{-1}$, $C_f = C_s/K_{sf}$, $f_s = M_s/(M_s^o + M_f^o)$, $f_m = M_m/(M_s^o + M_f^o)$, $f_f = M_f/(M_s^o + M_f^o)$, and the identity $f_s + f_m + f_f = 1$ are substituted into Equation 27, the differential equation for the variation in the concentration of a trace element in the residual solid as a function of melt fraction removed becomes

$$\frac{dC_s}{df_m} = C_s\left[(1-K_{sm}^{-1}) + (1-K_{sf}^{-1})\frac{df_f}{df_m}\right]\left[1 - f_m + f_f(K_{sf}^{-1}-1)\right]^{-1}. \tag{28}$$

Solution of mass-balance equation and error analysis

If Equation 28 is integrated and C_s is found as a function of f_m and f_f, then C_m can be computed from the relation $C_m = C_s K_{sm}^{-1}$. The integrated form of Equation 28 reduces to the usual expressions (e.g., Shaw 1970) for the composition of residual solid and melts in fluid-absent fractional melting (see Appendix III). In the general case, Equation 28 must be solved numerically to account for variations in K_{sm}, K_{sf}, and df_f/df_m during fluid-present partial melting as discussed earlier for isobaric fractional crystallization. These parameters are not generally constant across a wide range of melt fractions and need to be calculated self-consistently by a thermodynamic method such as the MELTS algorithm of Ghiorso and Sack (1995). In the simplified case in which K_{sm}, K_{sf}, and df_f/df_m are constant, Equation 28 may be integrated analytically. Constant φ implies $f_f = f_f^o + \phi f_m$ where f_f^o represents the mass fraction of fluid present in the system just below the solidus (i.e., when $f_m = 0$, $f_s = f_s^o$, and $f_f = f_f^o$). Equation 28 may therefore be written:

$$\frac{dC_s}{df_m} = \frac{C_s[(1-K_{sm}^{-1}) + (1-K_{sf}^{-1})\phi]}{\left[1 - f_m + f_f((K_{sf}^{-1}-1)\right]}. \tag{29}$$

Equation 29 is integrated, subject to the initial condition that $C_s = C_s^o$ at $f_m = 0$. The trace-element balance for the system at the solidus is $C_{sys} = C_s^o\left(f_s^o(1-K_{sf}^{-1}) + K_{sf}^{-1}\right)$, which allows for fluid fraction f_f^o and fluid composition $C_f^o = C_s^o/K_{sf}$ at the solidus prior to partial melting. For constant K_{sm}, K_{sf}, and φ, the composition of a trace element in the residue after fraction of melt f_m has been removed is

$$\frac{C_s}{C_s^o} = \left(\frac{1-(1-K_{sf}^{-1})f_f^o + [(K_{sf}^{-1}-1)\phi - 1]f_m}{[1-(1-K_{sf}^{-1})f_f^o]}\right)^{\frac{(1-K_{sm}^{-1})+(1-K_{sf}^{-1})\phi}{(K_{sf}^{-1}-1)\phi-1}}. \tag{30}$$

The corresponding expressions for the instantaneous melt composition (C_m) and the average of all melt increments (i.e., the aggregate melt composition, $\hat{C}_m$) along the melting path from the solidus ($f_m = 0$) to f_m are

$$\frac{C_m}{C_s^o} = K_{sm}^{-1}\left(\frac{1-(1-K_{sf}^{-1})f_f^o + [(K_{sf}^{-1}-1)\phi - 1]f_m}{[1-(1-K_{sf}^{-1})f_f^o]}\right)^{\frac{(1-K_{sm}^{-1})+(1-K_{sf}^{-1})\phi}{(K_{sf}^{-1}-1)\phi-1}} \tag{31}$$

and

$$\frac{\hat{C}_m}{C_s^o} = \frac{[(1-K_{sf}^{-1})f_f^o - 1]}{f_m}\left[\left(1 + \frac{[(K_{sf}^{-1}-1)\phi - 1]f_m}{(1-(1-K_{sf}^{-1})f_f^o}\right)^{\frac{-1}{K_{sm}[(K_{sf}^{-1}-1)\phi-1]}} - 1\right] \tag{32}$$

The expression for the instantaneous fluid phase composition is

$$\frac{C_f}{C_s^o} = K_{sf}^{-1}\left(\frac{1-(1-K_{sf}^{-1})f_f^o + [(K_{sf}^{-1}-1)\phi - 1]f_m}{[1-(1-K_{sf}^{-1})f_f^o]}\right)^{\frac{(1-K_{sm}^{-1})+(1-K_{sf}^{-1})\phi}{(K_{sf}^{-1}-1)\phi-1}}. \tag{33}$$

The error introduced by neglect of trace-element partitioning into the fluid during fluid-present fractional melting is easy to compute. The fractional error in the concentration of trace element in the melt is

$$\frac{C_m^{3\Psi} - C_m^{2\Psi}}{C_m^{3\Psi}} = 1 - \left(1 - f_m\right)^{K_{sm}^{-1}-1} \left(\frac{1-(1-K_{sf}^{-1})f_f^o}{1-(1-K_{sf}^{-1})f_f^o + [(1-K_{sf}^{-1})\phi - 1]f_m}\right)^{\frac{[(K_{sm}^{-1}-1)-(1-K_{sf}^{-1})\phi]}{[(K_{sf}^{-1}-1)\phi-1]}}. \tag{34}$$

In Figure 4, which represents a case of 10% fractional melting, the absolute value of the percent error, incurred by assuming that fluid-phase, trace-element partitioning has no effect on the melt composition, is portrayed; calculation details are provided in the figure caption. Once again, it is clear that failure to account for partitioning of elements, especially if they are fluid soluble, results in melt concentration errors that are large. For example, an incompatible element characterized by a bulk solid-melt partition coefficient of $K_{sm} = 0.01$ exhibits a 40% error for $K_{sf} = 0.1$ (somewhat soluble), and a 100% error for $K_{sf} = 0.01$ (soluble). Perusal of the data compiled in Electronic Appendix 1 (see also Fig. 8) indicates that, depending on the mineral assemblage of

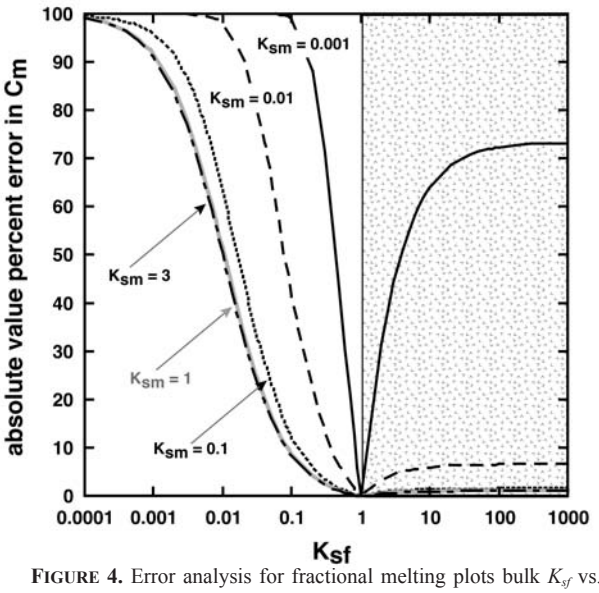

FIGURE 4. Error analysis for fractional melting plots bulk K_{sf} vs. absolute value percent error in C_m, based on Equation 34. Results shown for $f_m = 0.10$ (10% fractional melting); $\varphi = -0.10$; $f_f^0 = 0.01$ (i.e., source has 1% H_2O); range of K_{sm} from 0.001 to 3. Stippled region denotes negative values of percent error (i.e., $C_m^{3\Psi} < C_m^{2\Psi}$). Note that percent error for $K_{sf} = 1$ is 0 for all K_{sm}. Thus, $K_{sf} = 1$ yields solution that is equivalent to fluid-absent conditions.

the source (e.g., peridotitic, eclogitic, gabbroic, granodioritic, etc.), many elements fall into the category where the bulk $K_{sf} < 1$, and in some cases, bulk K_{sf} is << 1.

Graphical results

In this section, we show results based Equation 29, which gives the instantaneous composition of melts derived by fractional melting. In the case of fluid-present melting, both f_f^0 (the initial mass of fluid) and φ are important. In Figure 5, melt compositions are plotted for trace elements spanning a range of geochemical behaviors, from highly incompatible ($K_{sm} = 0.001$), moderately incompatible ($K_{sm} = 0.1$), to compatible ($K_{sm} = 1, 3$) for $f_f^0 = 0.01$ (e.g., 1% H_2O in the source) and $\varphi = -0.1$. The calculation is run until the $f_f = 0$, at which point the discrete fluid phase ceases to exist. For f_f^0, this transition occurs at $f_m = 0.1$ (i.e., 10% melting). For each K_{sm}, a range of K_{sf} is shown, from highly soluble (10^{-5}) to moderately insoluble (10). Examination of Figure 5a shows that for a highly incompatible element, K_{sf} values as large as 10^{-2} produce significant deviations from the fluid-absent case. For example, for $K_{sf} = 10^{-2}$, the normalized concentration of trace element can be orders of magnitude higher after 2% melting, compared to the fluid-absent case. Recall that in the case of a highly incompatible element, for fluid-absent fractional melting, the element is efficiently stripped from the solid source as melting progresses. Thus, at very small degrees of partial melting, normalized concentrations can be quite high, but as melting progresses, concentrations decrease significantly. Figure 5a also reveals that in cases in which elements are more soluble (e.g., 10^{-3} or less), the deviation from fluid-absent behavior is significant. For example, at as little as 4% melting, the normalized concentration is significantly enriched, compared to the source initial composition (over an order of magnitude) and compared to the predicted composition in the fluid-absent case (many orders of magnitude). Thus, in cases where fluid-present melting occurs but is not correctly assessed, there is potential for gross misinterpretation of the character of the source(s) and/or the mechanisms of melting for elements that are soluble. Elemental behavior at the point of transition from fluid-present to fluid-absent is best shown in Figures 5b, 5c, and 5d. For highly soluble elements, these plots show that, compared to the fluid-absent case, normalized concentrations can be orders of magnitude higher at the f_m at which $f_f \rightarrow 0$. For example, Figure 5b shows that the normalized concentration of a moderately incompatible but highly soluble element will change by several orders of magnitude at the fluid-present, fluid-absent transition (i.e., 10% melting). These figures also underscore how trace-element ratios, so often used in geochemical and petrologic analysis, may also be impacted. For any two elements i and j that have similar K_{sm} but very different K_{sf} (i = soluble, j = insoluble), progressive melting will fractionate these elements (i.e., i/j will increase dramatically); analysis neglecting this effect leads to significant interpretative misunderstandings. These results highlight the critical need to correctly assess the trace-element effects of fluid partitioning during melting.

Figure 6 illustrates results for the same parameters except φ = –0.2, which means twice as much fluid is removed for each increment of melt formation. The fraction of melt at which $f_f = 0$ is 0.05. In cases where K_{sf} is 1 or greater, φ = –0.2 has little to no impact on trace-element trends, compared to φ = –0.1 (e.g., compare results for Fig. 5 and 6, cases in which $K_{sf} = 1, 10$). For similar degrees of melting (at f_m less than where $f_f = 0$), the φ = –0.2 case generally yields normalized concentrations that are slightly higher than the φ = –0.1 case because, all other parameters being equal, more of the trace element has been transferred via the fluid when φ = –0.2. The critical issue to appreciate from Figures 5 and 6 is that the contribution that soluble elements make to the trace-element signature of partial melt during fluid-present melting must be properly characterized; otherwise, completely inaccurate conclusions may be drawn about source features and melting processes. Although not shown, results for integrated melt compositions ($\hat{C}_m$), perhaps a more widely applicable geochemical model than perfect fractional melting, yield the same conclusion.

SOLID-FLUID-MELT TRACE-ELEMENT PARTITIONING: THEORY AND EXPERIMENTAL DATA

A compilation of trace element mineral-fluid (K_{sf}) and fluid-melt (K_{mf}) partition coefficients from experimental studies is presented in Electronic Appendix 1. The compilation is representative, not exhaustive, and focuses upon recent studies. Most measurements have been made with pure H_2O as the solvent although a few studies have included dilute alkali halide aqueous fluids. Insofar as trace metal chloride species can be stable entities in aqueous solutions, the solubilty of some trace elements will depend significantly on chloride molality. The stability of such complexes at elevated conditions of pressure and temperature (e.g., at subduction zone depths) is largely unknown. Our purpose is to provide a summary that is useful for geochemical calculations involving common trace elements

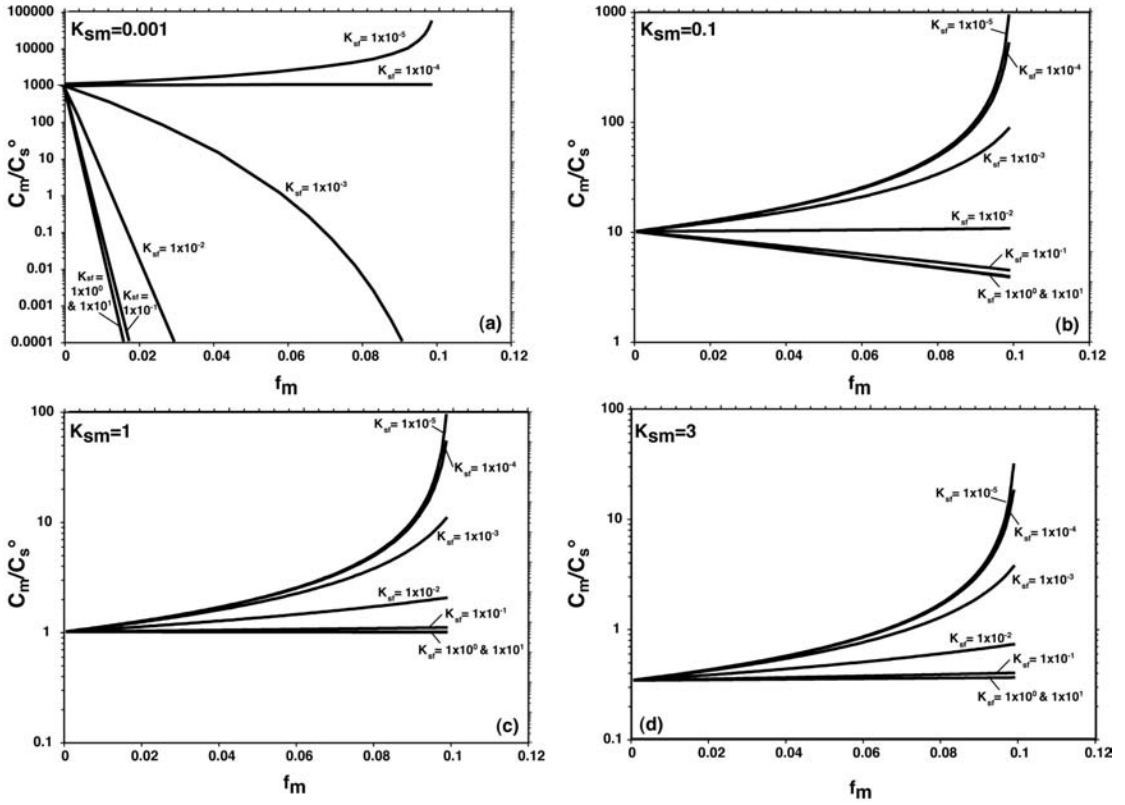

FIGURE 5. Plots depicting behavior of normalized trace element concentration (C_m/C_s^o) vs. f_m for fractional melting; φ = –0.10 and f_f^o = 0.01 (i.e., source has 1% H_2O). In all plots, K_{sf} = 1 illustrates system behavior for fluid-absent conditions. (**a**) Curves illustrating C_m/C_s^o trends for K_{sm} = 0.001 and K_{sf} of 10^{-5} to 10. (**b**) K_{sm} = 0.1 and K_{sf} of 10^{-5} to 10. (**c**) K_{sm} = 1.0 and K_{sf} of 10^{-5} to 10. (**d**) K_{sm} = 3 and K_{sf} of 10^{-5} to 10. Calculations stopped at f_m = 0.1 because this is the limit of fluid-present melting for this case.

found in important igneous phases. Potential mantle fluids span a wide range of compositions including water-rich fluids, concentrated brines, CO_2-rich fluids, and second critical point fluids (e.g., Bureau and Keppler 1999; Kessel et al. 2005). Halogen and sulfur-bearing compounds (e.g., HCl, HF, SO_2, H_2S, COS, etc.) may also be important components of mantle and crustal fluids. Similarly, the oxidation state of the fluid is important because of its effect on the speciation of fluids in the system H-O-C-S-Halogens. With so much potential variability in fluid composition and fundamental ignorance of the thermodynamic and electrostatic properties of water-rich, carbonic, and second critical point fluids, we recognize that a simple set of partition coefficients serves only as a rough guide. Even the electrostatic properties of pure water, quantitatively the most significant volatile constituent, are uncertain at conditions of high pressure and low temperature (900–1500 K) common in subduction environments. Despite the absence of a complete theory for calculation of the solubility of silicate, oxide, and other crystalline phases in geofluids at elevated temperature and pressure, some elementary considerations provide a means for rationalization of observed solid-fluid (K_{sf}) partition coefficients. The discussion presented here is most relevant to aqueous dipolar fluids for which the theory of electrolytes is most applicable. The thermodynamics of second critical point geofluids and the calculation of mineral solubility at elevated temperature and pressure represent important areas for further research. Here, only a brief synopsis is presented and a few generalizations made.

Water is an excellent solvent because its dipolar nature (high dielectric constant) permits solutes to exist as solvated positive and negative ions. The hydration or solvation shell of water molecules is essential in lowering the energy of the ions or polyions making dissolution reactions spontaneous although the degree of dissolution varies widely. The Gibbs energy of dissolution of a trace element in a solid is a balance of contributions from sublimation, ionization, and solvation (hydration). The individual contributions to the dissolution free energy can be appreciated by following the thermodynamic cycle implied by dissolution of a solid into its constituent ions or polyions. Consider Rb in alkali feldspar, $RbAlSi_3O_8$ where for brevity $X^- = (AlSi_3O_8)^-$ is the quasi-polyanion. The dissolution reaction may be decomposed according to the thermodynamic cycle:

$$RbX_s \rightarrow RbX_g \qquad \Delta G_{sublimation}$$
$$RbX_g \rightarrow Rb_g^+ + X_g^- \qquad \Delta G_{ionization}$$
$$Rb_g^+ \rightarrow Rb_{aq}^+ \qquad \Delta G_{solvation}$$
$$X_g^- \rightarrow X_{aq}^- \qquad \Delta G_{solvation}$$
$$\overline{RbX_s \rightarrow Rb_{aq}^+ + X_{aq}^- \qquad \Delta G_{dissolution}}$$

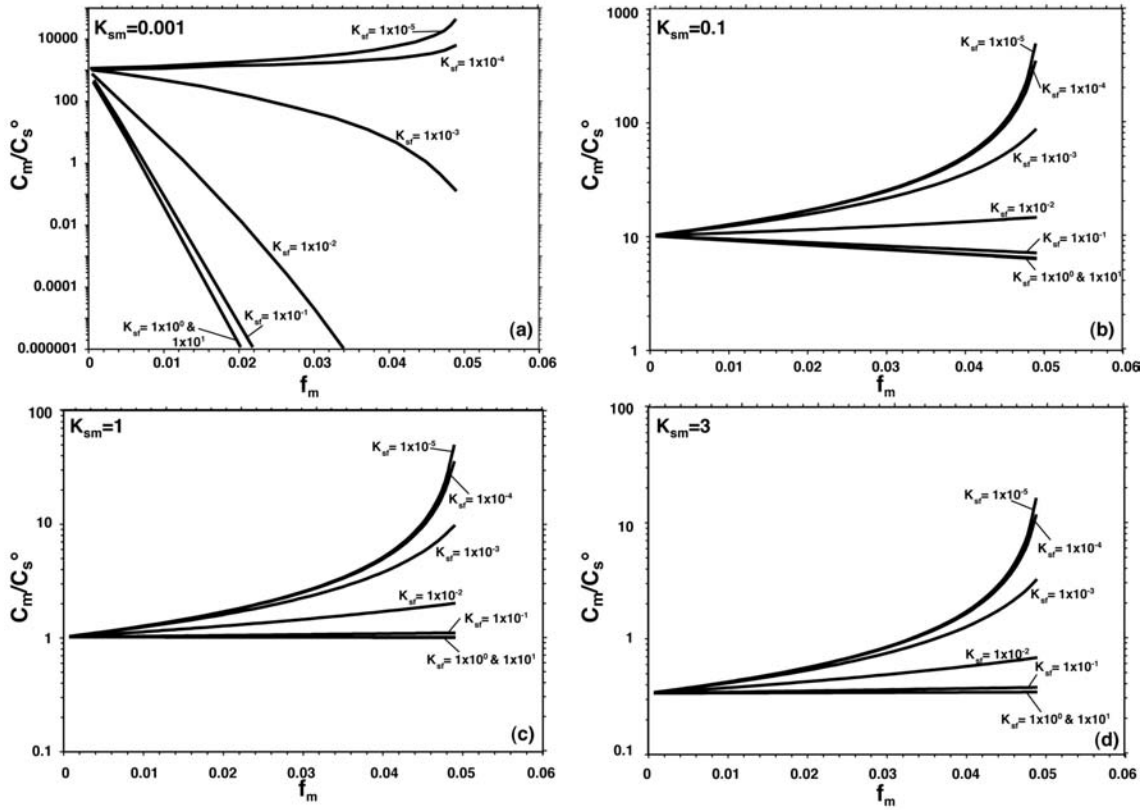

FIGURE 6. Plots depicting behavior of normalized trace element concentration (C_m/C_s^o) vs. f_m for fractional melting; $\varphi = -0.20$ and $f_f^o = 0.01$ (i.e., source has 1% H_2O). In all plots, $K_{sf} = 1$ illustrates system behavior for fluid-absent conditions. (**a**) Curves illustrating C_m/C_s^o trends for $K_{sm} = 0.001$ and K_{sf} of 10^{-5} to 10. (**b**) $K_{sm} = 0.1$ and K_{sf} of 10^{-5} to 10. (**c**) $K_{sm} = 1.0$ and K_{sf} of 10^{-5} to 10. (**d**) $K_{sm} = 3$ and K_{sf} of 10^{-5} to 10. Calculations stopped at $f_m = 0.05$ because this is the limit of fluid-present melting for this case.

The Gibbs energy of the dissolution reaction evidently includes contributions from sublimation, ionization, and solvation. The sum of the ionization and sublimation energies represents the lattice Gibbs energy of the crystalline solid containing the trace element. Hence $\Delta G_{dissolution} = \Delta G_{lattice} + \Delta G_{solvation}$ (Rb^+, aq) + $\Delta G_{solvation}$ (X^-, aq). The Gibbs energy of the dissolution reaction is related to the equilibrium solubility of the trace element according to $RT \ln K_{sf} = \Delta G_{diss}$. If activity coefficients are set to unity, then the equilibrium constant can be identified with the solid-fluid partition coefficient K_{sf}.

The solubility of a trace element is determined by the relative balance of the lattice Gibbs energy and the Gibbs energy of ion solvation. The Coulomb-Born ionic model for a crystalline solid is a useful construct to establish the first-order role played by cation charge and size. In that model, the 0 K lattice internal energy is directly proportional to the charge of the cation and inversely proportional to the cation-oxygen bond distance and hence the cation ionic radius ($\Delta E_{0K} \propto \frac{z_{cat}}{r_{cat}}$). The 0 K lattice internal energy is always positive and increases as the cation charge and size increase and decrease, respectively. The magnitude of the lattice Gibbs energy is smaller than the lattice internal energy because the entropy change associated with dissociation and sublimation is always positive. In general, a large positive lattice Gibbs energy will disfavor dissolution. In contrast, the solvation Gibbs energy of an ion is always negative. The Gibbs energy of hydration can be estimated from the Born model

$$\Delta G_{\text{solvation}} = \frac{-z^2 e^2 N_A}{8\pi\varepsilon_o r_{eff}}\left(1 - \frac{1}{\varepsilon_r}\right) \tag{35}$$

where z is the cation valance, e is the electron charge, N_A is Avogadro's number, ε_o is the permittivity of free space, ε_r is the relative permittivity (dielectric constant) of H_2O, and r_{eff} is the effective radius of the solvated (hydrated) ion or polyion. In the Born approximation, the solvent (i.e., H_2O) is treated as a uniform fluid of constant relative permittivity (dielectric constant), and the ion is treated as a charged sphere of effective radius r_{eff} defined as the distance from the center of the ion to the center of the water dipole. The solvation radius is proportional to but larger than the ionic radius of the trace element (approximately proportional to the crystal ionic radius) and is a function of fluid density (or pressure) and temperature. At fixed temperature and pressure, the solvation Gibbs energy is strongly negative for small, highly charged ions in media of high relative permittivity. The solvation Gibbs energy therefore scales as

$$\Delta G^{\circ}_{\text{solvation}} \propto \frac{z^2}{r_{eff}}\left(\frac{1}{\varepsilon_r} - 1\right)$$

where ε_r is a function of pressure and temperature (e.g., Pitzer 1983; Haar et al. 1984; Franck et al. 1990). Of the common species in magmatic fluids, H_2O offers the best solvent properties due to its relatively large dipole moment. Values for the relative

permittivity of some polar and non-polar geofluids may be found in Franck et al. (1990) and in Dandurand and Schott (1992). Small amounts of non-polar volatiles (e.g., CO_2 or CH_4) can have a relatively large effect on the dielectric constant of the fluid mixture. For example, addition of 10 mol% CO_2 to H_2O at 673 K and 0.1 GPa reduces the value of ε_r by a factor of three using the mixing rules of Looyenga (1965). This has the effect of decreasing the absolute value of the Gibbs solvation energy and hence reduces the trace-element concentration, other factors remaining constant. The higher the dielectric constant of a fluid, the better the neutralization of the force field between two atoms on the surface of the solid in contact with the fluid and hence, the greater its solubility. Scaling of solubility relations based on the Born solvation and Born-Coulomb lattice energy models outlined above gives $\log m \propto -\varepsilon_r^{-1}$, where m is the molality (moles of trace element per kg H_2O) of the trace element and ε_r is the dielectric constant of the mixed fluid. This expectation can be tested using experimentally determined solute content of oxides in H_2O and H_2O-CO_2 fluids measured by Schneider and Eggler (1986). They noted that the solubility of many cations in H_2O-CO_2 fluids ($w_w^f \approx 0.9$) in equilibrium with peridotites at ~2 GPa and 1100 °C is less by a factor of ~ 4 (from 12 wt% total solute to 3 wt% total solute) compared to those in pure H_2O at the same conditions of pressure and temperature. The dielectric constant of pure water decreases with increasing temperature due to thermal randomization of oriented dipoles. In contrast, increasing pressure favors ordering of dipoles and hence increases ε_r (Franck et al. 1990; Wasserman et al. 1995; Floriano and Nascimento 2004; Guàrdia and Marti 2004; Weingärtner and Franck 2005; Cai et al. 2005). Water, therefore, maintains its capacity to dissolve solids at depths along the geotherm and is an especially good solvent in "old" slabs at depth where temperatures are relatively low. The solubility of many trace elements in silicates and oxides increases as the aqueous fluid becomes more chloride-rich (Keppler 1996), reflecting the effects of ion association (complex formation). Recall that seawater has an equivalent molality of ~0.5 NaCl; many geologic fluids are considerably more saline. Further experimental work should address the issue of trace metal complex formation in chloride-bearing aqueous solutions. This may be very relevant to subduction zone magmatism.

From the point of view of trace-element geochemistry, the traditional way of assessing the solubilty of a trace element is to consider its field strength, defined $E_{fs} = \frac{z_{cat}}{R_i^2}$, where z_{cat} is the charge of the cation and R_i is the ionic radius of the cation. In light of the complexities of the dissolution process, E_{fs} is, at best, a rather crude way to systematize the solubility of trace elements in aqueous geofluids. In Figure 7, electric field strength is plotted for several elements arranged by atomic number using the compilation of Emsley (1991). One can distinguish four groupings of elements based on relative field strengths. The lowest-field-strength elements (which tend to be most soluble) are K, Rb, and Cs followed by Li, Na, Sr, Ba, and Pb, which in turn are followed by the Ca, Cu, Y, Mo, Sn, REE, Th, and U. Note that multiple oxidation states are shown for Ce and U. The high-field-strength elements include Be, B, Ti, V, Ni, Zr, Nb, Hf, Ta, and W. These elements are generally relatively insoluble except for the low atomic number elements Be and B, which have fairly low mineral-fluid partition coefficients for garnet- and clinopyroxene-fluid (Electronic Appendix 1). The anomalous high solubility of Be and B, despite their high field strengths, may be related to their small size and low coordination number with oxygen in crystalline silicates, low hydration numbers in aqueous solution, and the stability of oxide and halogen polyatomic ions involving Be and B.

Figure 8 summarizes values of K_{sf} for the minerals apatite, amphibole, micas, potassium feldspar, olivine, clinopyroxene, plagioclase, and garnet for all elements reported in Electronic Appendix 1. Recall that a low value of K_{sf} for a particular trace element implies that the element is relatively soluble in an H_2O-rich fluid. For mineral-fluid pairs in which multiple experimental results are available, we have plotted the geometric mean of all experimental values of K_{sf} for the given mineral-fluid pair. As an inset, we also show the minimum value of K_{sf}. For trace elements most relevant to problems in igneous petrology, Figure 8 shows that elements Cs, Rb, Ba, Pb, Sr, Mo, Th, Tb, Yb, U, Ce, Be, and B are moderately to highly soluble in phases such as clinopyroxene, garnet, plagioclase, and olivine. Thus, when these phases are quantitatively important, assessment of the fluid role in crystallization and melting is critical. Although there are sufficient experimental data on values of K_{sf} to at least partly evaluate the role of solid-fluid and melt-fluid trace-element partitioning, more experiments are needed to fully characterize mineral-fluid partitioning under the range of pressure, temperature, and fluid composition conditions relevant to mantle and crustal processes. An aspect that is particularly important to note is that experiments have shown that elements can become increasingly soluble in more saline/chloride-rich fluids (e.g., Holland 1972; Flynn et al. 1978; Keppler 1996; Reed et al. 2000). Because most of the experiments used to construct Figure 8 (see also Electronic Appendix 1) were run at low salinity or in pure water, this suggests that the solubility of many of these elements may be greater than shown here, thus underscoring the importance of including fluids in any trace-element evaluation. The minimum values marked on the inset to Figure 8 may therefore be more realistic when performing geochemical calculations. The experiments of Keppler (1996) illustrate this effect rather clearly and are plotted in Figure 9. He determined K_{sf} between clinopyroxene and pure H_2O and between clinopyroxene and a 5 molal (Na,K)Cl aqueous solution. For many elements, there is an order-of-magnitude difference in K_{sf} such that the solubility of a given trace element is greater in the chloride-bearing solutions compared to pure H_2O.

Figure 10 summarizes the geometric mean of the partition coefficient between fluid and melt (K_{fm}) for several melts, most of which are silicic. Most values of K_{fm} range between 0.01 and 10. Based on the identity $K_{sm}/K_{sf} = K_{fm}$, values of $K_{fm} \geq 0.01$ to 0.1 will be significant for analysis of trace-element distribution during fractional crystallization and fractional melting. Thus, like results discussed above for K_{sf}, many elements (e.g., Rb, K, Ba, Sr, Li, Th) will be quantitatively partitioned into co-existing supercritical fluid.

Summary and implications

Expressions to calculate trace-element partitioning in solid-melt-fluid systems subject to fractional and equilibrium crystallization and melting are presented in this paper. In general, a

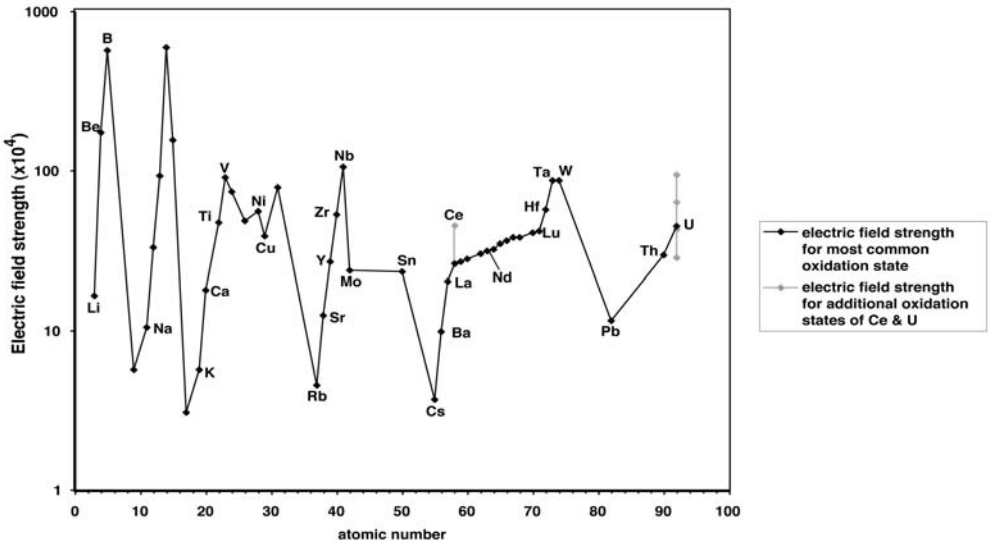

FIGURE 7. Atomic number vs. electric field strength ($\times 10^4$). Electric field strength shown for multiple oxidation states for Ce (+3, +4) and U (+3, +4, +5, +6); single oxidation state shown for all other elements. Elements can be grouped into four categories of electric field strength. Note general correlation between solubility in aqueous fluid and low values of electric field strength. See text for discussion.

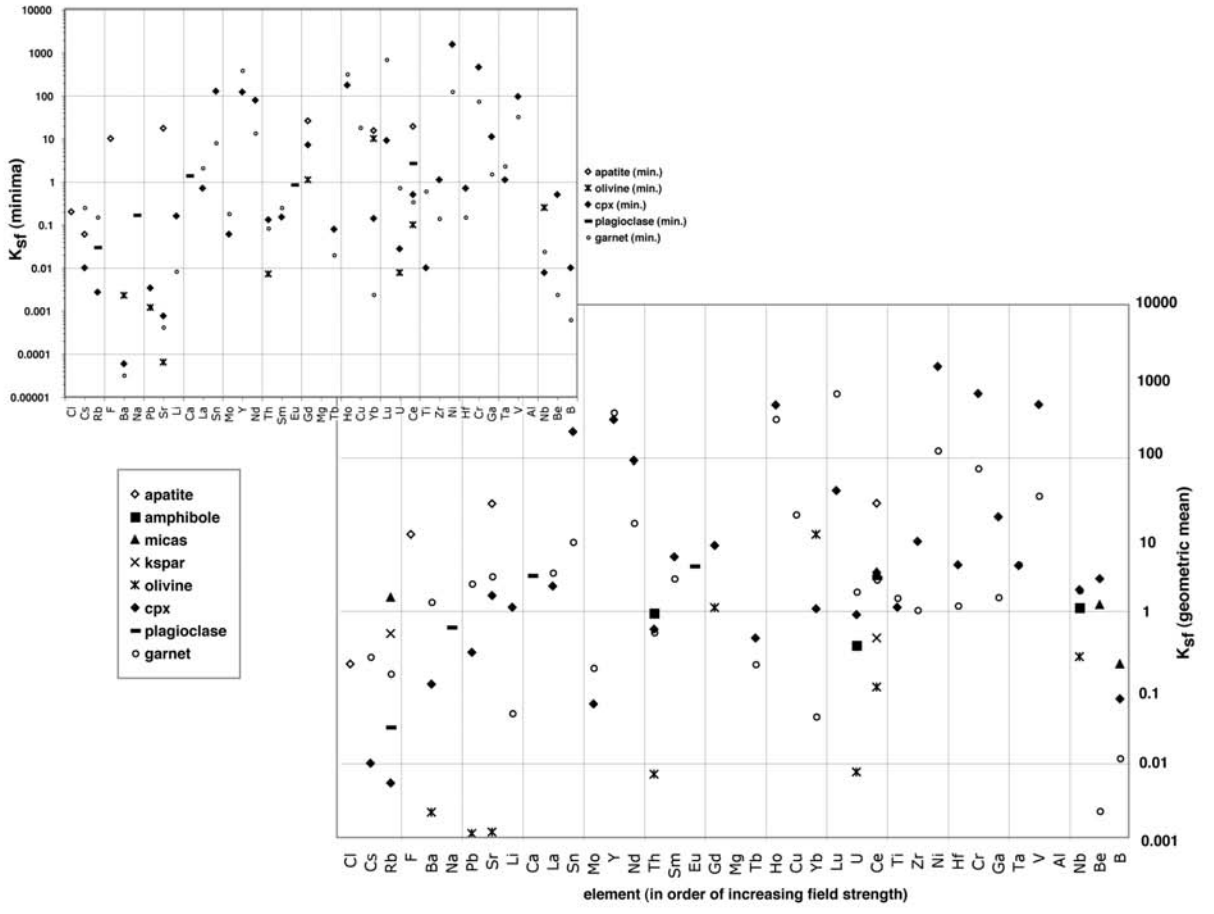

FIGURE 8. Solid-fluid partition coefficients (K_{sf}) for a range of elements, presented in order of increasing electric field strength, for the minerals apatite, amphibole, mica, potassium feldspar, olivine, clinopyroxene, plagioclase, and garnet. In cases where more than one datum is available, symbol represents geometric mean. Inset shows lowest K_{sf} for each mineral. Individual K_{sf} data, experimental conditions, and references can be found in Electronic Appendix 1.

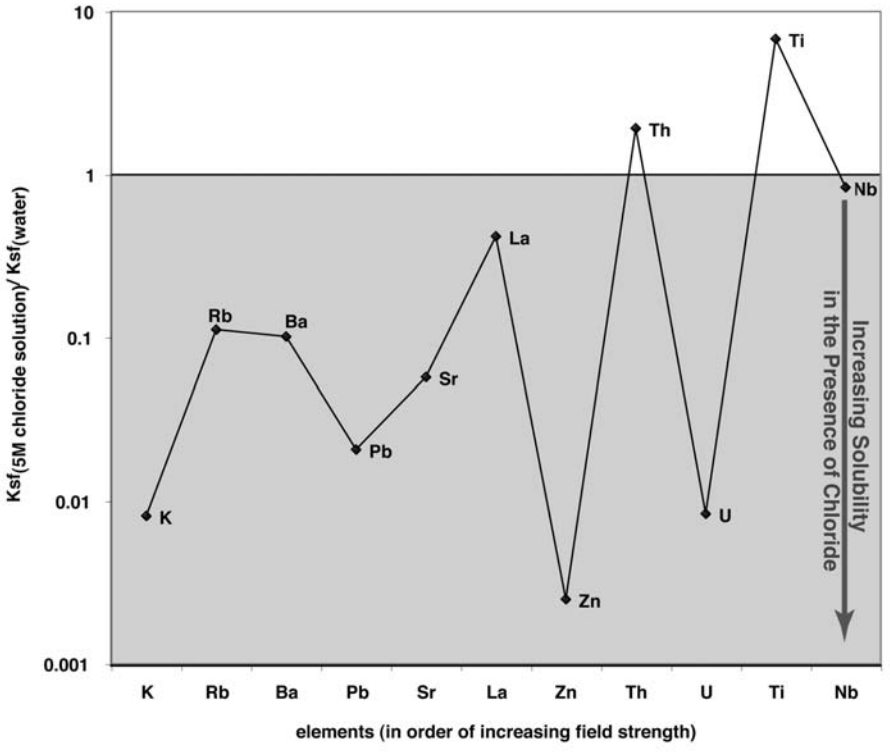

FIGURE 9. Elements in order of increasing electric field strength vs. ratio of K_{sf} in 5 *M* (Na,K)Cl solution to K_{sf} in pure water for selected trace elements in clinopyroxene. Data from Keppler (1996). Note many elements (e.g., K, Rb, Ba, Pb, Sr, U) experience an order-of-magnitude (or greater) increase in solubility in the presence of chloride-bearing solution. Nb experiences almost no change, and Th and Ti become less soluble in the chloride-bearing solution.

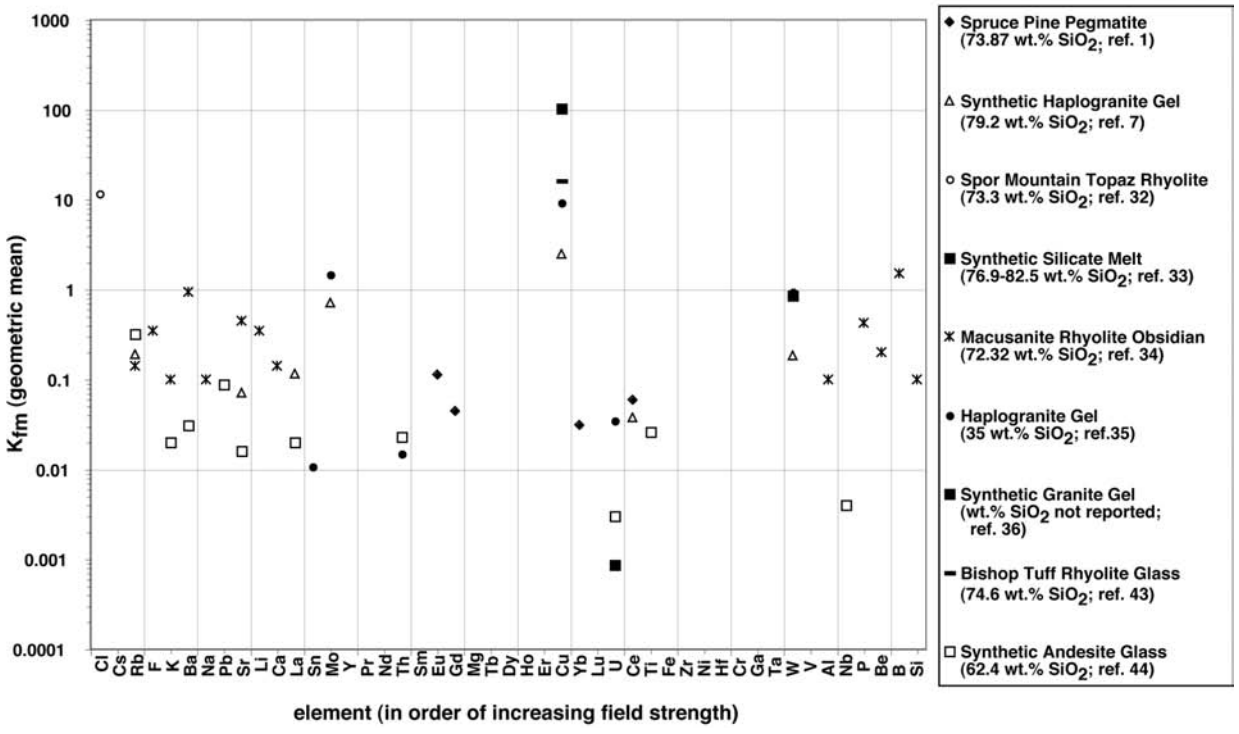

FIGURE 10. Fluid-mineral partition coefficients (K_{fm}) for a range of compositions; most are silicic. In cases where more than one datum is available, symbol represents geometric mean. Individual K_{fm} data, experimental conditions, and references can be found in Electronic Appendix 1.

coupled set of differential equations must be solved to model any process because the solubility of volatile components is dynamically partitioned between melt and fluid during phase transitions, and hence the variation of the fraction of fluid with fraction of melt is not a constant. For the limiting conditions of (1) constant partition coefficients (K_{sf} and K_{sm}); (2) H_2O present as the sole volatile constituent; and (3) water solubility independent of temperature and melt composition, we provide analytical solutions for instantaneous trace-element concentrations for solid, melt and fluid phases, and relevant average trace-element concentrations applicable to isobaric fractional crystallization and isobaric fractional and melting. Forward modeling results for the closed form solutions, informed by a compilation of K_{sf} and K_{fm} data (Electronic Appendix 1), clearly show significant differences between fluid-present and fluid-absent trace-element concentrations for soluble elements. Errors predicted for such element concentrations in fluid-present vs. fluid-absent cases can exceed 100% for geologically relevant scenarios. The range of K_{sf} and K_{fm} reported in the literature is large, and the magnitude of the effect of fluid-present crystallization and melting underscores the need that exists for additional K_{sf} and K_{fm} experimental measurements and progress in the thermodynamic theory of element solubility at elevated temperature and pressure. Measurements of the dielectric properties of possible mantle and crustal fluids are especially pertinent.

Although in this paper we have focused on providing the equations and partition coefficient data to address fluid-present trace-element calculations for melting and crystallization, the broader implications of our results are critical to appreciate. Since the formalism for quantifying the role of trace elements (Gast 1968; Schilling and Winchester 1967) was elucidated decades ago, trace-element concentrations and ratios have been used to both qualitatively and quantitatively describe magma-chamber processes (e.g., fractional crystallization, assimilation, recharge), melting processes (e.g., fractional, dynamic, continuous, equilibrium), character of source (e.g., source heterogeneity, plume structure), and involvement of various reservoirs or components in the origin of particular types of magmas (e.g., contributions from subducted lithosphere, continental crust, asthenosphere). It is also clearly established that many magmas are fluid-saturated for at least part of their history. Equations and analysis presented here yield the conclusion that in cases where interpretations derive from elements that are soluble, such as Rb, Ba, Sr, Th, U, Pb, and possibly even the REE, serious potential misinterpretation about source(s), processes, and even timescales (e.g., U-Th-Ba disequilibria) may result by not properly incorporating trace element behavior of fluid-saturated systems. Addition of these equations to the trace-element geochemist's "tool box" would seem to be a critical and essential step forward in the ongoing effort to provide sound and holistic, thermodynamically based descriptions of magmatic systems.

Acknowledgments

This material is based upon work supported by the National Science Foundation under Grants EAR 0609680, 0440010 to F.J.S., W.A.B., and M.S.G. Any opinions, findings, and conclusions or recommendations expressed in this material are those of the author(s) and do not necessarily reflect the views of the National Science Foundation. F.J.S. also acknowledges support from the U.S. Department of Energy. The comments of Paul Asimow, Don Baker, and two anonymous reviewers are gratefully acknowledged.

References cited

Albarède, F. (1995) Introduction to geochemical modeling, 543 p. Cambridge University Press, New York.

Allègre, C.J. and Minster, J.F. (1978) Quantitative models of trace element behavior in magmatic processes. Earth and Planetary Science Letters, 38, 1–25.

Allègre, C.J., Treuil, M., Minster, J.F., Minster, B., and Albarède, F. (1977) Systematic use of trace element in igneous petrology. Contributions to Mineralogy and Petrology, 60, 57–75.

Berger, A., Engi, M., and Burri, T. (2006) Tectonically controlled water flow and water assisted melting in the middle crust: Tertiary migmatites in the Southern Steep Belt of the Central Alps. Geophysical Research Abstracts, 8, 04604.

Brenan, J.M., Shaw, H.F., Ryerson, F.J., and Phinney, D.L. (1995). Mineral-aqueous fluid partitioning of trace elements at 900 °C and 2.0 GPa; constraints on the trace element chemistry of mantle and deep crustal fluids. Geochimica et Cosmochimica Acta, 59, 3331–3350.

Bureau, H. and Keppler, H. (1999) Complete miscibility between silicate melts and hydrous fluids in the upper mantle: Experimental evidence and geochemical implications. Earth and Planetary Science Letters, 165, 187–196.

Burnham, C.W. (1979) The importance of volatile constituents. In H.S. Yoder, Jr., Ed., The evolution of the igneous rocks; fiftieth anniversary perspectives, p. 439–482. Princeton University Press, New Jersey.

Cai, Y.Q., Mao, H.-K., Chow, P.C., Tse, J.S., Ma, Y., Patchkovskii, S., Shu, J.F., Struzhkin, V., Hemley, R.J., Ishii, H., Chen, C.C., Jarrige, I., Chen, C.T., Shieh, S.R., Huang, E.P., and Kao, C.C. (2005) Ordering of hydrogen bonds in high-pressure low-temperature H_2O. Physical Review Letters, 94, 1–4.

Campbell, I.M. and Taylor, S.R. (1983) No water, no granite—no oceans, no continents. Geophysical Research Letters, 10, 1061–1064.

Candela, P.A. (1989) Felsic magmas, volatiles, and metallogenesis. Reviews in Economic Geology, 4, 223–233.

Dandurand, J.L. and Schott, J. (1992) Prediction of ion association in mixed-crustal fluids. Journal of Physical Chemistry, 96, 7770–7777.

Defant, M.J. and Drummond, M.S. (1990) Derivation of some modern arc magmas by melting of young subducted lithosphere. Nature, 347, 622–665.

Elliott, T. (2003) Tracers of the Slab. In J. Eiler, Ed., Inside the subduction factory, 138, p. 23–45. American Geophysical Union, Washington, D.C.

Emsley, J. (1991) The elements, second edition, 251 p. Clarendon Press, Oxford.

Floriano, W.B. and Nascimento, M.A.C. (2004) Dielectric constant and density of water as a function of pressure at constant temperature. Brazilian Journal of Physics, 34(1), 38–41.

Flynn, R.T., Burnham, C.W., Drake, M.J., and Holloway, J.R. (1978) An experimental determination of rare earth partition coefficients between a chloride containing vapor phase and silicate melts. Geochimica et Cosmochimica Acta, 42(6A), 685–702.

Franck, E.U., Rosenzweig, S., and Christoforakos, M. (1990) Calculation of the dielectric constant of water to 1000 °C and very high pressures, Berichte der Bunsen-Gesellschaft, 94, 199–203.

Gast, P.W. (1968) Trace element fractionation and the origin of tholeiitic and alkaline magma types. Geochimica et Cosmochimica Acta, 32(10), 1057–1086.

Ghiorso, M.S. and Sack, R.O. (1995) Chemical mass transfer in magmatic processes; IV, A revised and internally consistent thermodynamic model for the interpolation and extrapolation of liquid-solid equilibria in magmatic systems at elevated temperatures and pressures. Contributions to Mineralogy and Petrology, 119(2–3), 197–212.

Grove, T.L. and Parman, S.W. (2004) Thermal Evolution of the Earth as recorded by komatiites. Earth and Planetary Science Letters, 219, 173–187.

Guàrdia, E. and Marti, J. (2004) Density and temperature effects on the orientational and dielectric properties of supercritical water. Physical Review E, 69 (011502), 1–11.

Haar, L., Gallagher, J.S., and Kell, G.S. (1984) NBS/NRC Steam Tables. Hemisphere Publishing Co., New York.

Holland, H.D. (1972) Granites, Solutions, and base metal deposits. Economic Geology and the Bulletin of the Society of Economic Geologists, 67(3), 281–301.

Kelemen, P.B., Yogodzinski, G.M., and Scholl, D.W. (2003) Along-strike variations in the Aleutian Island Arc: Genesis of High Mg# Andesite and implications for continental crust. In J. Eiler, Ed., Inside the Subduction Factory, 138, p. 223–276. American Geophysical Union, Washington, D.C.

Keppler, H. (1996) Constraints from partitioning experiments on the composition of subduction-zone fluids. Nature, 380, 237–240.

Kessel, R., Schmidt, M.W., Ulmer, P., and Pettke, T. (2005) Trace element signature of subduction-zone fluids, melts and supercritical fluids at 120–180 km depth. Nature, 437, 724–727.

Litasov, K., Ohtani, E., Langenhorst, F., Yurimoto, H., Kubo, T., and Kondo, T. (2003) Water solubility in Mg-perovskites and water storage capacity in the lower mantle. Earth and Planetary Science Letters, 211, 189–203.

Looyenga, H. (1965) Dielectric constant of heterogeneous mixtures. Physica, 31, 401–404.

Minster, J.F., Minster, J.B., Treuil, M., and Allègre, C.J. (1977) Systematic use of trace elements in igneous petrology. Contibutions to Mineralogy and Petrol-

ogy, 61, 49–77.
McCulloch, M.T. and Gamble, J.A. (1991) Geochemical and geodynamical constraints on subduction zone magmatism. Earth and Planetary Science Letters, 102, 358–374.
Ohtani, E., Litasov, K., Hosoya, T., Kubo, T., and Kondo, T. (2004) Water transport into the deep mantle and formation of a hydrous transition zone. Physics of the Earth and Planetary Interiors, 143–144, 255–269.
Pitzer, K.S. (1983) Dielectric constant of water at very high temperature and pressure. Proceedings of the National Academy of Sciences, 80, 4575–4576.
Plank, T. and Langmuir, C.H. (1998) The chemical composition of subducting sediment: Implications for the crust and mantle. Chemical Geology, 145, 325–394.
Prouteau, G., Scaillet, B., Pichavant, M., and Maury, R.L. (1999) Fluid-present melting of ocean crust in subduction zones. Geology, 27(12), 1111–1114.
Reed, M.J., Candela, P.A., and Piccoli, P.M. (2000) The distribution of rare earth elements between monzogranitic melt and the aqueous volatile phase in experimental investigations at 800 °C and 200 MPa. Contributions to Mineralogy and Petrology, 140(2), 251–262.
Schilling, J.G. and Winchester, J.W. (1967) Rare-earth fractionation and magmatic processes. In S.K. Runcorn, Ed., Mantles of the Earth and terrestrial planets, p. 267–283. Interscience Publishers, New York.
Schneider, M.E. and Eggler, D.H. (1986) Fluids in equilibrium with peridotite minerals: Implications for mantle metasomatism. Geochimica et Cosmochimica Acta, 50, 711–724.
Shaw, D.M. (1970) Trace element fractionation during anatexis. Geochimica et Cosmochimica Acta, 34, 237–242.
——— (1978) Trace element behaviour during anatexis in the presence of a fluid phase. Geochimica et Cosmochimica Acta, 42(6A), 933–944.
Stalder, R., Foley, S.F., Brey, G.P., and Horn, I. (1998) Mineral-aqueous fluid partitioning of trace elements at 900–1200 °C and 3.0–5.7 GPa; new experimental data for garnet, clinopyroxene, and rutile, and implications for mantle metasomatism. Geochimica et Cosmochimica Acta, 62(10), 1781–1801.
Stern, R.J. (2002) Subduction zones. Reviews of Geophysics, 40, 1–37.
Tatsumi, Y. (2005). The subduction factory: How it operates on Earth. GSA Today, 15, 4–10.
Wasserman, E., Wood, B., and Brodholt, J. (1995) The static dielectric constant of water at pressures up to 20 kbar and temperatures to 1273 K; Experiment, simulations and empirical equations. Geochimica et Cosmochimica Acta, 59(1), 1–6.
Weingärtner, H. and Franck, E.U. (2005) Supercritical water as a solvent. Angewandte Chemie International Edition, 44, 2672–2692.
White, S.M., Crisp, J.A., and Spera, F.J. (2006) Long-term volumetric eruption rates and magma budgets. Geochemistry, Geophysics, Geosystems—G^3, 7(Q03010), 20 p.

Manuscript received May 25, 2006
Manuscript accepted June 12, 2007
Manuscript handled by Don Baker

Appendix I

In this appendix, we show that Allègre et al. (1977) made the approximation of neglecting the presence of the fluid phase in the material balance expression for trace-element partitioning between melt, fluid, and solid. The derivation of their result begins on p. 64 of Allègre et al. (1977). Because their equations are not numbered, we have assigned them sequential labels (A, B, C, ...) for reference. We use the variable symbols defined in our paper since there is a one-to-one mapping with those used by Allègre et al. (1977). Numbered equations are those derived in the text of this paper.

Equations B and C represent definitions of the partition coefficients applicable when crystallized solids and exsolved fluids are fractionated from the melt. The expressions are

$$\frac{dm_f}{dM_f} = K_{fm}\frac{m_m}{M_m} \tag{B}$$

and

$$\frac{dm_s}{dM_s} = K_{sm}\frac{m_m}{M_m}. \tag{C}$$

Recall that $C_m = m_m/M_m$ and that lower case refers to the mass of a trace element and upper case refers to the mass of a phase. Subscripts s, f, and m refer to solid, fluid, and melt phases, respectively. Now, Allègre et al. (1977) followed Holland (1972), and assume that the solubility of the volatile component (e.g., H_2O) in the melt is constant. For isobaric fractional crystallization, this is only approximately valid. Although temperature and melt composition (and hence the solubility of H_2O) change during fractional crystallization, the largest effect on water solubility is pressure, a constant during isobaric fractionation. The more-precise way to handle this issue is to couple a phase-equilibria model (such as MELTS, Ghiorso and Sack 1995) to the trace elements. For purposes of illustration in this Appendix, we accept this approximation. Allègre et al. (1977) Equation D on p. 64 reads

$$dM_f = -GdM_m \tag{D}$$

where we have added a minus sign to the right hand side (RHS) of their expression since G, the water solubilty, is positive and dM_m is negative during crystallization when fluid is exsolved (i.e., dM_f is positive). Equation D implies (if we assume that melt is water saturated) that as crystallization proceeds and the mass of melt (M_m) decreases by increment dM_m, the mass of fluid phase M_f increases by –G dM_m. Equation D does not hold exactly if crystallizing solids contain structural H_2O or hydroxyl although, unless copious amounts of hydrous phase fractionate, the bulk of the H_2O remains in the melt rather than in coexisting solid(s). The total amount of a trace element taken out of magma is (top of p. 65)

$$-dm_m = dm_s + dm_f. \tag{F}$$

That is, a trace element is removed by crystallization of solid and exsolution of fluid.

Substitute B and C into F and find

$$-dm_m = K_{fm}\frac{m_m}{M_m}dM_f + K_{sm}\frac{m_m}{M_m}dM_s. \tag{AI-1}$$

Now substitute D into AI-1 and find

$$-dm_m = -K_{fm}\frac{m_m}{M_m}G\,dM_m + K_{sm}\frac{m_m}{M_m}dM_s. \tag{AI-2}$$

Allègre et al. (1977) did not give Equation AI-2. Instead, the final result they gave is

$$dm_m = (K_{sm} + K_{fm}G)\,m_m\frac{dM_m}{M_m}. \tag{G}$$

The only way to get from Equation AI-2, which is formally correct, to the result of Allègre et al. (1977) is to ignore the presence of the fluid phase. That is, to go from Equation AI-2 to Equation G, Allègre et al. (1977) assumed by neglecting the mass of the fluid phase that $M_s + M_m = M_{total}$. Then one finds $dM_s = -dM_m$ and Equation AI-2 becomes

$$dm_m = K_{fm}\frac{m_m}{M_m}G\,dM_m + K_{sm}\frac{m_m}{M_m}dM_m, \tag{AI-3}$$

which is identical to Equation G of Allègre et al. (1977). However, the total mass balance is not $M_s + M_m = M_{total}$ as assumed by Allègre et al. (1977), but instead $M_s + M_s + M_f = M_{total}$. This latter form is the one used in this study. Finally, we point out that Allègre et al. (1977) clearly recognized the approximate nature of

their derivation. On p. 65 immediately below their derivation they say "Note that the gas phase is not considered as an additional phase." The derivation we present in the text explicitly allows for the presence of the fluid phase and hence differs fundamentally from that presented by Allègre et al. (1977).

Appendix II

We show in the text that treating the fluid phase as the equivalent of another solid phase is a special case of the general treatment of simultaneous solution to Equations 10 and 13. In the case of solid–melt crystal fractionation involving multiple simultaneously fractionating phases at an invariant point where the mass ratios of fractionating solids are constant, the procedure is to define a phase mass-weighted partition coefficient (the bulk partition coefficient) and to use the analytical form of the Rayleigh fractionation expression. Consider crystal fractionation of an n+2 phase system made up of n solids ($s1$, $s2$, ... sn), a fluid phase, and a melt phase. The expression analogous to text Equation 11 is

$$\frac{d\ln C_m}{d\ln f_m}=\left[(K_{s1m}-1)+(K_{s1m}-K_{s2m})\frac{df_{s2}}{df_m}+\ldots(K_{s1m}-K_{sn})\frac{df_{sn}}{df_m}+(K_{s1m}-K_{fm})\frac{df_f}{df_m}\right]. \quad \text{(AII-1)}$$

Partition coefficients are defined in the usual way; note that $K_{fm} = C_f/C_m = \frac{\bar{K}_{sm}}{K_{sf}}$. Here we explore the implications of treating melt-fluid trace-element partitioning identically to the way one treats solid-melt partitioning when multiple crystalline phases are present. To proceed, the total derivatives appearing on the RHS of Equation AII-1 must be determined. This is accomplished by noting that f_m is a function of the mass fractions of all n solids ($f_{s1}, f_{s2}, ..f_{sn}$) and the fluid phase (f_f):

$$f_m = F(f_{s1}, f_{s2},\ldots f_{sn}, f_f) \quad \text{(AII-2)}$$

and then expanding in differential form:

$$df_m=\left(\frac{\partial f_m}{\partial f_{s1}}\right)_{f_{s2},\ldots f_{sn},f_f}df_{s1}+\left(\frac{\partial f_m}{\partial f_{s2}}\right)_{f_{s1},f_{s3}\ldots f_{sn},f_f}df_{s2}+\ldots+\left(\frac{\partial f_m}{\partial f_{sn}}\right)_{f_{s1},f_{s2}\ldots fs(n-1),f_f}df_{sn}+\left(\frac{\partial f_m}{\partial f_f}\right)_{f_{s1},f_{s2}\ldots f_{sn}}df_f. \quad \text{(AII-3)}$$

The mass-balance relation gives the condition:

$$\sum_{\varphi=1}^{n} f_\varphi + f_f + f_m = 1 \quad \text{(AII-4)}$$

where ϕ is summed over all crystalline phases. From Equation AII-4, values for the partial derivatives are found:

$$\left(\frac{\partial f_m}{\partial f_{s1}}\right)_{fs2,\ldots,f_{sn},f_f}=\left(\frac{\partial f_m}{\partial f_{s2}}\right)_{fs1,\ldots,f_{sn},f_f}=\ldots\left(\frac{\partial f_m}{\partial f_{sn}}\right)_{fs1,f_{s2}\ldots f_f}=\left(\frac{\partial f_m}{\partial f_f}\right)_{fs1,f_{s2}\ldots f_{sn}}=-1 \quad \text{(AII-5)}$$

Combining Equation AII-3 and Equation AII-5, the needed total derivatives are found:

$$\frac{df_m}{df_{s1}}=-1\left(1+\frac{df_{s2}}{df_{s1}}+\ldots\frac{df_{sn}}{df_{s1}}+\frac{df_f}{df_{s1}}\right)$$
$$\frac{df_m}{df_{s2}}=-1\left(\frac{df_{s1}}{df_{s2}}+1+\ldots\frac{df_{sn}}{df_{s2}}+\frac{df_f}{df_{s2}}\right) \quad \text{(AII-6)}$$
$$\frac{df_m}{df_{sn}}=-1\left(\frac{df_{s1}}{df_{sn}}+\frac{df_{s2}}{df_{sn}}+\ldots1+\frac{df_f}{df_{sn}}\right)$$
$$\frac{df_m}{df_f}=-1\left(\frac{df_{s1}}{df_f}+\frac{df_{s2}}{df_f}+\ldots\frac{df_{sn}}{df_f}+1\right).$$

For the bulk partition concept to apply, the ratios of all fractionating phases (including the fluid phase) are in constant proportion to one another. That is, the following conditions must hold:

$$f_{s2}/f_{s1} = Z_2, fs_3/f_{s1} = Z_3, \ldots f_{sn}/f_{s1} = Z_n \text{ and } f_f/f_{s1} = \text{constant} = Z_f. \quad \text{(AII-7)}$$

The Z's are all constants in Equation AII-7. The derivatives required for evaluation of Equation AII-1 are determined using Equations AII-6 and AII-7 and are

$$\frac{df_m}{df_{s2}}=-\left(Z_2^{-1}+1+\frac{Z_3}{Z_2}+\ldots+\frac{Z_{sn}}{Z_2}+\frac{Z_f}{Z_2}\right)$$
$$\frac{df_m}{df_{sn}}=-\left(Z_{sn}^{-1}+\frac{Z_2}{Z_{sn}}+\frac{Z_3}{Z_{sn}}+\ldots+1+\frac{Z_f}{Z_2}\right) \quad \text{(AII-8)}$$
$$\frac{df_m}{df_f}=-\left(Z_f^{-1}+\frac{Z_2}{Z_f}+\ldots+\frac{Z_{sn}}{Z_f}+1\right).$$

The derivatives in Equation AII-8 are all constant. This means that the term inside the square brackets of Equation AII-1 involves only the ratios of the mass fractions of the fractionating phases (including the fluid) and the constant partition coefficients. Hence the RHS of Equation AII-1 is a constant and can be written in the $K_B - 1$ form when the fluid phase is treated identically to any other phase present but with the appropriate partition coefficient K_{fm}. How does this treatment relate to the one developed in the text? In particular, under what circumstances are the two forms equivalent? Because it is assumed that the ratios of all fractionating phases are in constant proportion, Equations AII-4 and AII-7 imply that

$$f_f = [1+Z_f^{-1}(1+Z_2+\ldots+Z_{sn})]^{-1} - f_m[1+Z_f^{-1}(1+Z_2+\ldots+Z_{sn})]^{-1}. \quad \text{(AII-9)}$$

Equation AII-9 can be differentiated and rearranged to give

$$\frac{df_f}{df_m}=\frac{-Z_f}{1+Z_2+Z_3+\ldots+Z_{sn}}. \quad \text{(AII-10)}$$

Equation AII-10 can be compared to Equation 13 from the text. Clearly, these two equations are different because the RHS of Equation AII-10 is strictly a constant whereas this is not the case for text Equation 13.

As noted in the text, df_f/df_m must be computed according to an internally consistent phase-equilibria model (e.g., MELTS). In the simpler case when H_2O is the sole volatile component and when the solubility of water is constant independent of temperature and melt composition, then the approximation $df_f/df_m = -S_w = \varphi$ holds where S_w, the solubility of water in the melt, is constant. In this case, and only in this case, one finds

$$Z_f = (1 + Z_2 + Z_3 + \ldots + Z_{sn})S_w. \quad \text{(AII-11)}$$

That is, the two models are equivalent provided the ratio of the mass fraction of fluid to the mass fraction of solid number 1 is related to the constant water solubility and the mass ratios for the other solids according to Equation AII-11.

Appendix III

The following derivation illustrates that the fluid-present fractional melting equations reduce to the classical Rayleigh equations in the fluid-absent case. When no free supercritical fluid phase is present during fractional melting, the following conditions are applicable: $K_{sf} \rightarrow \infty$, $K_{sf}^{-1} \rightarrow 0$, $df_f/df_m = 0$ and $f_f = 0$. Hence Equation 28 assumes the form:

$$\frac{dC_s}{df_m} = \frac{C_s[(1-K_{sm}^{-1})]}{(1-f_m)}. \quad \text{(AIII-1)}$$

Equation AIII-1 is integrated according to

$$\int_{C_s^o}^{C_s} \frac{dC_s}{C_s} = (1-K_{sm}^{-1}) \int_0^{f_m} \frac{df_m}{(1-f_m)}. \quad \text{(AIII-2)}$$

This leads to the final form for the concentration of a trace element in the residual solid:

$$\frac{C_s}{C_s^o} = (1-f_m)^{(K_{sm}^{-1}-1)}. \quad \text{(AIII-3)}$$

Using the definition of the solid-melt partition coefficient, $K_{sm} = C_s/C_m$, the instantaneous concentration of a trace element in the melt when the melt fraction f_m has been removed is:

$$\frac{C_m}{C_s^o} = K_{sm}^{-1}(1-f_m)^{(K_{sm}^{-1}-1)}. \quad \text{(AIII-4)}$$

This result is identical to the form given in standard references such as Shaw (1970) or Albarède (1995) for the composition of fractional melt in solid-melt systems with constant partition coefficient. The fluid-present expressions are clearly a generalization of the more-limited case of fluid-absent fractional melting.

Appendix IV

Expressions for the instantaneous and average compositions of solids, melt, and fluid in equilibrium crystallization and equilibrium melting in the presence of a free fluid phase are derived here. Although these cases have solutions for solid-melt systems (i.e., fluid-absent conditions), the valid expressions for fluid-present conditions, to our knowledge, have not been derived.

Shaw (1978) presented an analysis of trace-element behavior during fluid-present anatexis. His model was based upon the assumption that, during progressive fractional fusion, the ratio of fluid mass to residual solid mass ($M_f/M_s = f_f/f_s$) remains constant. This is clearly not the case: the effect of fractional melting, in fact, is to strongly dehydrate the residue because water is quite soluble in silicate melts, especially at elevated pressure. Consequently, although of historical interest, the treatment of Shaw is not applicable to fluid-present anatexis. Similarly, we are not aware of any general treatment of equilibrium crystallization in the presence of a fluid phase. It is therefore useful to provide explicit expressions for the trace-element concentrations in solid, melt, and fluid relevant to equilibrium partial melting and crystallization under isobaric conditions. Closed form solutions exist only for constant K_{sm} and K_{sf}. In the more-realistic case with variable partition coefficients, one must employ numerical solution of the relevant differential equations in consort with phase-equilibria computations (e.g., MELTS, Ghiorso and Sack 1995).

Fluid-present equilibrium crystallization

During equilibrium crystallization in the presence of a fluid phase, the melt, fluid, and solid maintain mutual equilibrium. The differential balance written in terms of the mass fractions of melt, solid and fluid is

$$d(C_s f_s + C_m f_m + C_f f_f) = 0. \quad \text{(AIV-1)}$$

Using the definitions of K_{sm} and K_{sf} and the total mass balance $f_f + f_m + f_s = 1$, one finds for the composition of the melt, solid, and fluid:

$$\frac{C_m}{C_m^o} = \left[f_m(1-K_{sm}) + K_{sm}(1-f_f) + f_f K_{sm}/K_{sf}\right]^{-1} \quad \text{(AIV-2)}$$

$$\frac{C_s}{C_m^o} = K_{sm}\left[f_m(1-K_{sm}) + K_{sm}(1-f_f) + f_f K_{sm}/K_{sf}\right]^{-1} \quad \text{(AIV-3)}$$

$$\frac{C_f}{C_m^o} = \frac{K_{sm}}{K_{sf}}\left[f_m(1-K_{sm}) + K_{sm}(1-f_f) + f_f K_{sm}/K_{sf}\right]^{-1}. \quad \text{(AIV-4)}$$

In equilibrium crystallization, the average composition of melt, solid, and fluid always equals the instantaneous composition.

Fluid-present equilibrium melting

Fluid-present equilibrium melting is closely related to fluid-present equilibrium crystallization. One small difference is that the initial condition in equilibrium melting involves specification of the fraction of fluid present at the solidus. The differential balance is

$$d(C_s f_s + C_m f_m + C_f f_f) = 0. \quad \text{(AIV-5)}.$$

Using the definitions of K_{sm} and K_{sf}, the total mass balance $f_f + f_m + f_s = 1$, and recognizing that the concentration of trace element in the system (C_{sys}) is constant during progressive fusion and equal to $C_{sys}^o = C_s^o[(1-K_{sf}^{-1})f_s^o + K_{sf}^{-1}]$, the expressions for the melt, solid, and fluid concentrations are

$$\frac{C_m}{C_{sys}^o} = \left[f_m(1-K_{sm}) + K_{sm}(1-f_f) + f_f K_{sm}/K_{sf}\right]^{-1} \quad \text{(AIV-6)}$$

$$\frac{C_s}{C_{sys}^o} = K_{sm}\left[f_m(1-K_{sm}) + K_{sm}(1-f_f) + f_f K_{sm}/K_{sf}\right]^{-1} \quad \text{(AIV-7)}$$

$$\frac{C_f}{C_{sys}^o} = \frac{K_{sm}}{K_{sf}}\left[f_m(1-K_{sm}) + K_{sm}(1-f_f) + f_f K_{sm}/K_{sf}\right]^{-1} \quad \text{(AIV-8)}.$$

Like equilibrium crystallization, there is no distinction between average and instantaneous concentrations.